Microscopic insight into properties and electronic instabilities of impurities in cubic and lower symmetry insulators: the influence of pressure

2006 J. Phys.: Condens. Matter 18 R315

(http://iopscience.iop.org/0953-8984/18/17/R01)

INSTITUTE OF PHYSICS PUBLISHING JOURNAL OF PHYSICS: CONDENSED MATTER

J. Phys.: Condens. Matter **18** (2006) R315–R360 doi:10.1088/0953-8984/18/17/R01

TOPICAL REVIEW

Microscopic insight into properties and electronic instabilities of impurities in cubic and lower symmetry insulators: the influence of pressure

M Moreno[1], M T Barriuso[2], J A Aramburu[1], P García-Fernández[1] and J M García-Lastra[2]

[1] Departamento de Ciencias de la Tierra y Física de la Materia Condensada, Universidad de Cantabria, 39005 Santander, Spain
[2] Departamento de Física Moderna, Universidad de Cantabria, 39005 Santander, Spain

Received 17 February 2006
Published 13 April 2006
Online at stacks.iop.org/JPhysCM/18/R315

Abstract

This article reviews the microscopic origin of properties due to transition-metal (TM) impurities, M, in insulator materials. Particular attention is paid to the influence of pressure upon impurity properties. Basic concepts such as the electronic localization in an MX_N complex, the electrostatic potential, V_R, arising from the rest of the lattice ions or the elastic coupling of the complex to the host lattice are initially exposed. The dependence of optical and magnetic parameters on the impurity–ligand distance, R, in cubic lattices is discussed in a first step. Emphasis is put on the actual origin of the R dependence of $10Dq$. Examples revealing that laws for strict cubic symmetry cannot in general be transferred to lower symmetries are later given. This relevant fact is shown to come from allowed hybridizations like nd–$(n + 1)$s as well as the influence of V_R. As a salient feature the different colour in ruby and emerald is stressed to arise from distinct V_R potentials in Al_2O_3 and $Be_3Si_6Al_2O_{18}$. The last part of this review deals with electronic instabilities. The phenomena associated with the Jahn–Teller (JT) effect in cubic lattices, the origin of the energy barrier among equivalent minima and the existence of coherent tunnelling in systems like MgO:Cu^{2+} are discussed. An increase of elastic coupling is pointed out to favour a transition from an elongated to a compressed equilibrium conformation. Interestingly the equilibrium geometry of JT ions in non-cubic lattices is shown to be controlled by mechanisms different to those in cubic systems, V_R playing again a key role. The relevance of first principles calculations for clarifying the subtle mechanisms behind off-centre instabilities is also pointed out. Examples concern monovalent and divalent TM impurities in lattices with the CaF_2 structure. The instability due to the transition from the ground to an excited state is finally considered. For complexes with significant elastic coupling vibrational frequencies and the Stokes shift are expected to undergo bigger changes through a chemical rather than a hydrostatic pressure.

The reduction of Huang–Rhys factors upon increasing the pressure is discussed as well.

(Some figures in this article are in colour only in the electronic version)

Contents

1. Introduction

This review deals with the *microscopic origin* of physico-chemical properties associated with impurities in insulating materials. Although the presence of impurities in a liquid or solid compound can sometimes be undesirable they are in other cases the source of interesting properties which are absent in the pure compound. In liquids the presence of solute molecules gives rise to phenomena like the osmotic pressure or the decrease of the freezing point. As regards solid compounds, impurities in iron and silicon are behind the industry of steel and electronic devices, respectively, while doped insulating materials are involved in solid state lasers [1, 2], scintillators [3–5], storage phosphors [6, 7], long-lasting phosphorescence displays [8] and also gemstones [9–11]. In this domain special interest is raised by impurity ions with an electronic *open shell* configuration or at least a first excited state lying in the optical region. Throughout this article special attention is paid to impurity ions whose *active* electrons are in the *valence* region, their optical and magnetic properties being thus particularly sensitive to the environment. Most of the analysed systems involve 3d and 4d transition-metal (TM) ions, although examples dealing with ns^1 impurities (like Tl^{2+} or Ag^0) will also be discussed.

From a basic standpoint there is an important difference between doped liquids and solids. In the former case, the configurational entropy related to the rapid motion of solute molecules in the solvent plays a key role for understanding microscopically a phenomenon like the osmotic pressure [12, 13]. In a liquid solvent the time required by a solute molecule for travelling a distance of 10 Å is about 10 ps, while in a doped crystalline solid well below the melting

point that time can be days or even years [14]. This fact stresses that impurities in crystalline solids can be viewed as anchored to a given lattice point. Therefore, in these cases only the rapid vibrations around the equilibrium position or quick jumps among different conformations contribute to the entropy and other thermodynamic functions.

Very different situations are experimentally found when truly diluted impurities in insulators are considered. Sometimes, the impurity replaces a host lattice ion keeping the local symmetry at least in the electronic ground state. This situation where only a *symmetric* distortion of neighbour ions happens is just found for divalent impurities like Ni^{2+} or Mn^{2+} in a cubic fluoroperovskite [15–20], or for Cr^{3+}- or Fe^{3+}-doped elpasolites [21–30]. However, there are other cases where the impurity remains *on-centre* in the electronic ground state but there is a non-symmetric distortion of neighbour ions leading to a reduction of the local symmetry. This behaviour appears, for instance, when a *static Jahn–Teller* (JT) effect is taking place, such as is found for d^9 or d^7 ion doped alkali halides, cubic perovskites or SrO [31–35].

The distortion of ligands and the subsequent lowering of local symmetry can also happen for ions *without* orbital degeneracy in the ground state. A good example of this possibility concerns Mn^{2+} in BaF_2 [36–39] where the local symmetry is T_d and not O_h as is found for isomorphous lattices like CaF_2 or SrF_2 [40].

An impurity does not necessarily occupy a site of the host lattice. This is observed, for instance, for hydrogen atoms in alkali halides [41] or CaF_2 [42] as well as for Cu^{2+}-doped NH_4X (X = Cl, Br) crystals grown from solutions where the impurity occupies an interstitial position [43–47]. The *off-centre* motions undergone by ions which are initially at on-centre positions also belong to this domain [48–57]. For instance, while Ni^{2+} in CaF_2 replaces a Ca^{2+} ion, it has been well proved by means of electron paramagnetic resonance (EPR) and electron nuclear double resonance (ENDOR) techniques that the Ni^+ ion formed after x-irradiation experiences a big off-centre displacement along ⟨100⟩ directions [50, 51]. This phenomenon, responsible for drastic changes of the coordination number and associated properties of the impurity, seems to be very subtle. In fact, it is observed for SrF_2:Cu^{2+} [56] but not for Cu^{2+}-doped CaF_2 [58]. Off-centre motions are also observed in cases like KCl:Li^+ and KBr:Cu^+ involving a closed shell impurity [59–61].

It is worth noting that the local geometry around an impurity can change significantly on passing from the ground to an electronic excited state. As an example, low-temperature luminescence spectra of Cr^{3+}-doped cubic elpasolites reveal the existence of progressions involving the Jahn–Teller mode e_g [21–25]. This fact just means that in the $^4T_{2g}$ first excited state (where active electrons are still localized) ligands display a tetragonal equilibrium geometry and not an octahedral one [62, 63]. In other cases, the excited state can be close to or just placed in the conduction band of the host lattice, leading to the appearance of an anomalous luminescence with a big Stokes shift [64, 65]. This situation is found for some divalent rare earth impurities like Sm^{2+} or Tm^{2+} but not for divalent 3d impurities like Mn^{2+} or Ni^{2+}. Such a different behaviour can be rationalized bearing in mind that the ionization potential for the former ions is around 23 eV while for Mn^{2+} it is equal to 33.7 eV [39, 64–67].

More complex situations can appear when an impurity is joined to another defect. So, in insulating lattices when an impurity ion M^{m+} replaces a host cation A^{n+}, complex defects involving vacancies can be formed when $m > n$ [41, 32]. In other cases, charge compensation occurs through the formation of a pair with another impurity. Well known cases are the formation of M^{3+}–O^{2-} (M = Fe, Yb) [68–76] or Pb^{2+}–OH^- [77] pairs in lattices like $KMgF_3$.

The presence of an impurity in a lattice breaks its translational symmetry. For this reason a deep understanding of properties due to a pure compound seems in principle to be easier than when impurities are introduced in it. Nevertheless, in the ground state of a pure insulating compound electrons are localized [78–81] and this situation often remains when a TM impurity

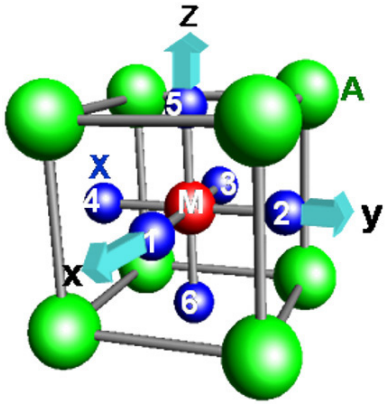

Figure 1. MX_N complex inserted into the $KMgF_3$ lattice.

is added. In the latter case active electrons coming from the impurity are usually (though not necessarily always) localized in the MX_N complex [82–84] formed by the impurity and the N nearest anions or ligands (figure 1). The existence of this strong electronic localization often allows one to understand the properties associated with an impurity in a given lattice by considering only clusters involving fewer than 100 atoms [85–88, 19, 30, 57]. This fact just points out that for properly explaining the properties of an impurity in an insulator it is not necessary to know the right wavefunction of the *whole* crystal. This idea is thus connected with the nearsightedness principle [89].

The search for a microscopic insight into properties coming from impurities in insulators thus involves several steps: (i) knowledge of the local structure in the electronic ground state; (ii) explanation of spectroscopic data (optical absorption maxima, EPR parameters, Raman peaks, etc) reflecting the local equilibrium geometry in the electronic ground state; (iii) changes of properties induced by variations of distances between the impurity and neighbour ions; (iv) relation between the local geometry of the ground state and its electronic structure; and (v) changes of the local structure on passing from the ground to an excited state and its influence on the luminescent emission and the Stokes shift.

While in pure crystalline compounds the structure is well determined by means of standard x-ray diffraction methods, such a technique is not useful for knowing the local structure around an impurity. The extended x-ray absorption fine structure (EXAFS) technique can currently provide good information about distances between the impurity and neighbour ions although usually with errors of at least 1 pm [90–92].

The advent of reliable theoretical calculations has favoured a better microscopic understanding of the five steps involved in the microscopic description of an impurity. Although *ab initio* calculations are able to reproduce reasonably well the *equilibrium* impurity–ligand distances and many spectroscopic parameters, the improvement introduced by calculations goes far beyond this step. In fact, calculations allow one to explore the electronic properties of a system in situations *far* from the equilibrium geometry, while experimental data on the ground state are usually obtained *at* such geometry. Moreover, by means of calculations performed for different electronic configurations and different basis sets it is much easier to clarify which *orbital* is the main one *responsible* for a given property [93, 94, 57]. Examples illustrating the importance of this procedure are offered in sections 3, 5 and 6.

Although the study on TM impurities in insulators is of interest in the research on deep centres in semiconductors [95] and active centres of proteins [96], it goes far beyond the domain of doped materials. Indeed, such an insight is also relevant for pure insulators where electrons

are localized in the ground state. To this domain first belong the so-called Mott–Hubbard and charge transfer insulators [97–99]. This kind of material should be metallic according to the traditional band theory based in the mean field approximation. However, this discrepancy is not surprising. Indeed, the dissociation limit of a simple molecule like H_2 is not well reproduced within such an approximated framework where the two electrons are allowed to be on the same atom even when interatomic distances are much higher than $\sim$1 Å [100]. It is worth noting now that many properties of a charge transfer insulator like NiO have been explained by considering NiO_6^{10-} clusters [99, 101–103]. Even the magnetic behaviour of this kind of compound has been accounted for by considering only clusters of fewer than 20 atoms [104, 105]. Along this line, the crystal field spectrum of $KNiF_3$ is found to be quite similar to that of $KMgF_3$:Ni^{2+} [15]. Therefore, this fact points out that many optical features of both systems can be basically understood *only* on the basis of the NiF_6^{4-} complex although in $KNiF_3$ such complexes are not isolated but ligands are shared [106].

An insight on the instabilities present in doped insulators can also shed some light on phase transitions and related phenomena in pure compounds. So, the knowledge of the interplay between electronic structure and local geometry for JT impurities can also be useful for explaining the structure in pure compounds with a cooperative JT effect [107–110]. Also some light on the origin of the ferroelectricity (present in insulating lattices like $BaTiO_3$) can be obtained through the study of off-centre motions experienced by impurities which convey the creation of a *local dipole* moment [111, 112]. In the same way, an understanding of the *dynamic* JT effect in doped cubic lattices [113] may be of help in the realm of manganites with colossal magnetoresistance [109, 114–116] and copper oxoperovskites displaying high-T_c superconductivity [117–119]. Finally the study of impurities centres can provide an insight into the nature of defects formed in pure insulators under x-irradiation [120]. For instance, the self-trapped hole formed in AgCl essentially corresponds to the $AgCl_6^{4-}$ complex [120–122], which is also found in chloride lattices containing Ag^{2+} impurities [31, 123]. Similarly, in pure $PbWO_4$ the electron is self trapped as a WO_4^{3-} complex [124, 125].

The present review is arranged as follows. Section 2 provides the basic theoretical framework for explaining the properties of TM impurities in insulators as well as a review of spectroscopic parameters. Section 3 deals with on-centre impurities in high-symmetry lattices. In these *model systems* particular attention is devoted to laws governing the dependence of spectroscopic parameters on the impurity–ligand distance, R, as well as their microscopic origin. The case of on-centre impurities but with lower local symmetry is dealt with in section 4, where the transferability of laws found for local cubic symmetry is analysed. Section 5 is focused on JT impurities. Aside from discussing all phenomena in cubic lattices arising from the JT interaction, attention is also paid to distortions on ligands produced in lattices which are not cubic and thus orbital degeneracy is broken [108, 126, 127]. In section 6, devoted to the microscopic origin of off-centre displacements, special attention is paid to underline the differences with the JT effect. Finally, the last section is concerned with symmetric and non-symmetric changes of the local geometry on passing from the ground electronic state to excited states. This issue is relevant as regards the Stokes shift which in turn partially controls the emission yield [128, 59, 39].

2. Impurities in insulators: basic concepts and spectroscopic parameters

2.1. Electron localization

As first pointed out by Kohn [78–81], the electronic density in the ground state of an insulating material is made of fragments which are disconnected and have essentially a localized character.

Table 1. Symmetry adapted linear combinations of p and s ligand orbitals. Coordinates are defined in figure 1. In octahedral symmetry σ bonding is present in the antibonding e_g orbital while in t_{2g} there is only π bonding. For this reason the two adapted linear combinations corresponding to e_g are sometimes referred to as $\chi_{p\sigma}$ and $\chi_{s\sigma}$.

		χ_p	χ_s
e_g	$3z^2-r^2$	$\frac{1}{\sqrt{12}}\{-2z(5)+2z(6)+x(1)+y(2)-x(3)-y(4)\}$	$\frac{1}{\sqrt{12}}\{2s(5)+2s(6)-s(1)-s(2)-s(3)-s(4)\}$
	x^2-y^2	$\frac{1}{2}\{-x(1)+y(2)+x(3)-y(4)\}$	$\frac{1}{2}\{s(1)-s(2)+s(3)-s(4)\}$
t_{2g}	xy	$\frac{1}{2}\{y(1)+x(2)-y(3)-x(4)\}$	
	xz	$\frac{1}{2}\{z(1)+x(5)-z(3)-x(6)\}$	
	yz	$\frac{1}{2}\{z(2)+y(5)-z(4)-y(6)\}$	

Usually the electronic structure of crystalline compounds is described in the framework of the mean field approximation and associated Bloch wavefunctions made from valence atomic orbitals. However, such wavefunctions have an itinerant rather than a localized character. In a simple insulating material like NaF all one-electron states of the valence band are filled. Nevertheless, in this situation such a description is *fully equivalent* to considering a Slater determinant composed of localized atomic or, more properly, Wannier wavefunctions [81, 100]. An aid for understanding this relevant result can be obtained by looking at the simple He_2 molecule [100]. Here, the molecular orbital (MO) description and the Heitler–London picture both give the same ground state wavefunction, while this is not the case for H_2 made of two non-closed shell atoms. This reasoning thus supports that a crystal like NaF can basically be viewed as composed of *ions*. In this material the valence band is mainly built from 2p valence orbitals of F^- ions while the conduction band roughly arises from empty 3s orbitals of Na^+ and its bottom is placed ∼0.2 eV below the zero level [129]. If the ionization potential of free F^- is $I_{0L} = 3.4$ eV [14] the centre of gravity of the valence band can be estimated to be at

$$\varepsilon_L = -I_{0L} - eV_A; \qquad V_A = \alpha e/R_H \tag{1}$$

where V_A means the Madelung potential at an anion site, e is the proton charge, and R_H the interatomic distance of the pure host lattice. The Madelung potential also plays an important role for understanding the properties of TM impurities. Let us consider a Ni^+ impurity placed at a cationic position in NaF. If I_{0M} denotes the ionization potential of the free impurity ion then the energy of the centre of gravity of the d levels can be estimated by

$$\varepsilon_M(d) = -I_{0M} - eV_C; \qquad V_C = -\alpha e/R_H. \tag{2}$$

In this case the Madelung energy $-eV_C$ at the cation site raises the d levels of the impurity. For NaF:Ni^+, using $I_{0M} = 18.1$ eV [130] and $-eV_C = 10.9$ eV, this simple estimation leads to $\varepsilon_M(d) \approx -7.5$ eV, implying that d levels lie above those coming from $2p(F^-)$. As the $3d^9$ Ni^+ ion has an open shell a transfer of electronic charge from F^- ions close to the impurity can be produced, implying that the total charge on the impurity, z_M, is smaller than its nominal charge, z_M^*. Within an MO framework in a cubic symmetry each $|d, \Gamma\rangle$ orbital of a free impurity ion has to be replaced by an antibonding MO:

$$|\psi, \Gamma\rangle = N\{|d, \Gamma\rangle - \lambda_p|\chi_p, \Gamma\rangle - \lambda_s|\chi_s, \Gamma\rangle\}. \tag{3}$$

Here $|\chi_p, \Gamma\rangle$ ($|\chi_s, \Gamma\rangle$) means a suitable linear combinations of p (s) valence orbitals of nearest anions or ligands belonging to the Γ irreducible representation (irrep) of the symmetry group of the centre [83]. The corresponding bonding orbitals also involve an admixture of ligand wavefunctions with appropriate $|d, \Gamma\rangle$ counterparts. Expressions for $|\chi_p, \Gamma\rangle$ and $|\chi_s, \Gamma\rangle$ corresponding to an octahedral unit are given in table 1. It is worth noting that for octahedral

complexes the ligand s–p hybridization is symmetry allowed for e_g antibonding levels but forbidden for t_{2g} orbitals. As in the ground state bonding orbitals are fully populated but there are holes in the antibonding levels this produces a transfer of electronic charge from closed shell ligands to the impurity. At the same time this process leads to a transfer of unpaired electron density from the impurity to ligands.

If Na^+ is replaced by a divalent TM impurity the flow of electronic charge from ligands tends to increase [131]. Considering the NaF:Mn^{2+} system, if $z_M = 1.75$ then the I_{0M} value is equal to 27 eV and thus $\varepsilon_I(d) \approx -16$ eV [84]. Nevertheless, the $Na^+ \rightarrow Mn^{2+}$ substitution leads to an inward relaxation of close anions [132], raising $\varepsilon_M(d)$ up to about -13 eV. This simple reasoning points out that mainly 3d levels of Mn^{2+} would lie well below the bottom of the conduction band of NaF. Because of this important fact, the flow of unpaired electron density is basically stopped on ligands and thus the electronic properties coming from the impurity can reasonably be explained solely in terms of the MX_N complex whose equilibrium distance is however influenced by the host lattice. This idea thus explains why the optical and EPR data of cubic fluoroperovskites doped with the same divalent impurity look very similar although they are not identical [15–20, 29, 133].

It should be noted that the flow of unpaired electron density beyond the complex region can happen not only when the host lattice gap, E_g, decreases but also in highly ionic materials. The latter situation can arise when the ground state of the impurity is lying close to the bottom of the conduction band. If this circumstance is rare for the ground state of divalent impurities in alkali and alkali earth halides [39], it is however found for KCl:Ag^0 involving a neutral impurity [134, 135]. If KCl ($E_g = 8.4$ eV [129]) is replaced by the more covalent AgCl compound ($E_g = 3.2$ eV [136]), a substitutional Ag^0 impurity at cationic sites seems to be electronically unstable [135]. In lattices like AgCl or AgBr there are impurity centres with an important electron delocalization which recalls that found for shallow impurities in semiconductors [122, 137, 138].

2.2. Spectroscopic parameters of impurity centres with cubic or tetragonal symmetry

For the sake of clarity let us recall the optical and magnetic parameters associated with MX_N molecules embedded in a high-symmetry host lattice. A more detailed discussion can be found in classical books on spectroscopy and ligand field theory [59, 83, 131, 139–141]. A typical one-electron diagram for the ground state of a MX_6 complex displaying cubic symmetry is shown in figure 2. Aside from the d–d or crystal field (CF) transitions in an MX_N complex, electron jumps from a full ligand level to an empty antibonding one are also possible, leading to the so-called charge transfer (CT) transitions [131]. In cubic symmetry crystal field multiplets are characterized by the Racah parameters B and C as well as by the cubic field splitting, $10Dq$, between antibonding e_g ($\sim 3z^2 - r^2$, $x^2 - y^2$) and t_{2g} ($\sim xy, xz, yz$) levels [83]. It is worth noting that the value of B and C parameters derived from experiments is usually smaller than B_0 and C_0 corresponding to the free impurity ion [83, 131, 139, 140]. This fact is an indirect consequence of the transfer of unpaired electron density described by equation (3). For a given impurity, the covalence increases following the decrement of optical electronegativity [131], thus implying that an MBr_N complex is more covalent than MF_N at normal pressure. By the same reason CT transitions are significantly red shifted along the series $MF_N \rightarrow MCl_N \rightarrow MBr_N$. The onset of CT transitions of MX_6^{4-} (M = Cu, Ag, Ni, Rh; X = Cl, Br) [142–144], $CrCl_6^{3-}$ [145] and $FeCl_6^{4-}$ [28] complexes lies in the optical region while that for CrF_6^{3-} [146, 147, 26] and $MnCl_6^{4-}$ [142, 143] complexes is at 64 000 and 58 000 cm^{-1}, respectively. A band peaked at 59 000 cm^{-1} in $NaMgF_3$ [148] can thus hardly be ascribed to a CT transition of an MnF_6^{4-} complex, but it could arise from a 3d $\rightarrow$ 4s transition [149].

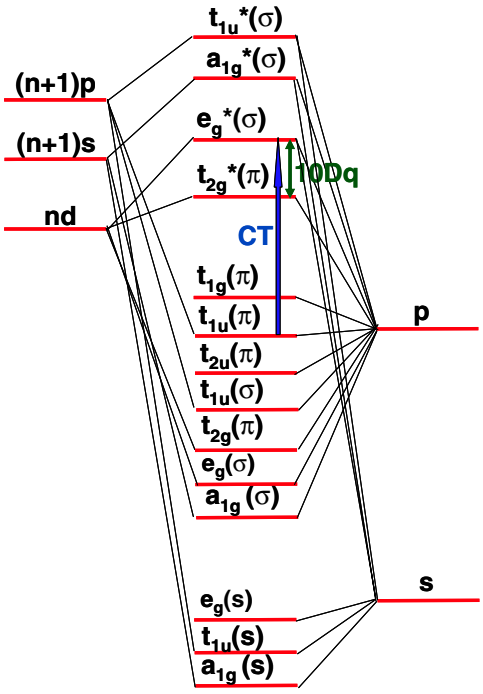

Figure 2. Molecular orbital diagram corresponding to an octahedral MX_N complex. Atomic levels of the transition-metal impurity, M, (ligand anions, X) are depicted on the left-hand (right-hand) side of the diagram. The crystal field splitting energy, $10Dq$, and one metal to ligand charge transfer (CT) transition are also shown.

As the CT transitions observed experimentally are electric dipole allowed they are usually more important than CF ones as regards the polarizability of the complex and thus its Raman activity [150]. The observation of local vibrations due to an MX_N complex in a host lattice through Raman spectroscopy is thus enhanced if the laser frequency can correspond to a CT transition [150–153].

A precise description of the localization of unpaired electrons and, at the same time, of the covalency in an MX_N complex in a host lattice can be obtained through EPR and ENDOR spectra. In fact, the spins of nuclei close to the unpaired electron density can be detected through such techniques. However, this task can hardly be achieved by means of usual optical measurements due to broadening of zero-phonon lines caused by unavoidable random strains [59, 150]. In the case of rare earth impurities this drawback has been overcome through the hole burning technique [153].

The experimental information derived from EPR is condensed in the effective spin Hamiltonian, H_s. For an $S = 1/2$ complex, a typical spin Hamiltonian is [139, 141]

$$H_s = \beta \mathbf{S}[\mathbf{g}]\mathbf{H} + \mathbf{S}[\mathbf{A}]\mathbf{I} + \sum_{l=1}^{N} \mathbf{S}[\mathbf{T}_l]\mathbf{I}_l. \tag{4}$$

The first and second terms in H_s mean the Zeeman and hyperfine contributions, respectively. The last term depicts the superhyperfine interaction with N ligand nuclei. As a salient feature, H_s should reflect the local symmetry of the impurity centre [139]. As [**g**] and [**A**] are second-order tensors they are reduced to only one diagonal component in cubic symmetry while in tetragonal symmetry the diagonalized [**g**] tensor involves two different components,

called $g_\parallel$ and $g_\perp$. For a *purely ionic* d^9 complex displaying an elongated octahedral geometry the expressions of $g_\parallel$ and $g_\perp$ are simply given by [139]

$$g_\parallel = g_0 + 8\xi_M/\Delta_{xy}; \qquad g_\perp = g_0 + 2\xi_M/\Delta_{xz,yz} \tag{5}$$

where Δ_{xy} just means the $xy \rightarrow x^2 - y^2$ CF excitation energy and ξ_M is the spin–orbit coefficient of the free d^9 ion. As $\Delta_{xy} \approx \Delta_{xz,yz}$, equation (5) predicts that $(g_\parallel - g_0)/(g_\perp - g_0)$ should be close to 4, provided bonding in the d^9 complex is ionic. Although experimental data on d^9 complexes with small or moderate covalency follow this rule [31], important departures appear in complexes where the unpaired electron spends more time on ligands [154]. A particular amazing situation is found for $CdBr_2{:}Ag^{2+}$ [155] and in irradiated $AgBr_{0.85}Cl_{0.15}$ [156] where EPR supports the formation of elongated $AgBr_6^{4-}$ complexes. In these cases the [**g**] tensor is found to be practically isotropic. For instance $g_\parallel = 2.072$ and $g_\perp = 2.067$ are measured for $CdBr_2{:}Ag^{2+}$ [155]. This surprising experimental fact can reasonably be understood by considering the following [154–157]: (i) the covalency (described by equation (3)) involved in the antibonding $\sim x^2 - y^2$ level where the unpaired electron is placed; (ii) the contribution of CT excitations to the [**g**] tensor, whose importance growths with the covalency of the bonding; (iii) the inclusion of the ligand spin–orbit interaction. It is worth noting that the spin–orbit coefficient, ξ_L, for a free ligand is just equal to $\xi_L = 2400\ cm^{-1}$ for Br^- which is a bit higher than $\xi_M = 1800\ cm^{-1}$ for free Ag^{2+} and about three times bigger than $\xi_M = 830\ cm^{-1}$ for free Cu^{2+}. The importance of CT excitations for explaining the experimental [**g**] tensor of other impurities has also been underlined [158–162].

More direct information on covalency is embodied in the superhyperfine interaction given in equation (4). The invariance of the whole superhyperfine interaction under the symmetry operations of the local symmetry group implies that any $[\mathbf{T}_k]$ tensor in equation (4) has to be invariant but only under the operations which do not modify the k ligand. In the case of octahedral (cubic) coordination this subgroup is C_{4v} (C_{3v}), thus implying that the diagonal $[\mathbf{T}_k]$ tensor involves two different components: $T_\parallel$ corresponds to the line joining the impurity and the k ligand and $T_\perp$ to the perpendicular plane. $T_\parallel$ and $T_\perp$ are usually written as

$$T_\parallel = A_s + 2A_{an}; \qquad T_\perp = A_s - A_{an}. \tag{6}$$

For octahedral complexes with unpaired σ electrons A_s mainly comes from the admixture of valence s orbitals of ligands in e_g orbitals, being thus proportional to λ_s^2 in equation (3) [83–139]. Calling λ_σ and λ_π the λ_p coefficients in equation (3) for e_g and t_{2g} orbitals, respectively, A_{an} depends in general on both λ_σ^2 and λ_π^2 quantities. For octahedral d^8 complexes, where there are only unpaired electrons in the e_g orbital, it is λ_σ^2 which mainly determines A_{an}. The relation between A_{an} and λ_σ^2 and λ_π^2 for a d^5 impurity is more complex in cubic than in octahedral coordination as in this case σ ligand levels are not along a $\langle 111 \rangle$ type direction but form an angle, θ_σ, with it [163]. Calculations are thus required for knowing this relevant quantity (which cannot be known from symmetry) for interpreting experimental A_{an} values.

The interpretation of the hyperfine tensor [**A**] associated with TM impurities requires us to go beyond the usual molecular orbital description where a filled orbital does not give rise to any contribution [139]. Let us consider, for instance, a d^5 ion like Mn^{2+} or Fe^{3+} in the high-spin configuration $^6A_{1g}$ under cubic symmetry, where the diagonal component of [**A**] is called simply A. For p and d electrons, the hyperfine interaction described in the effective Hamiltonian (4) comes only from the magnetic dipole term in the *real* Hamiltonian, involving orbital operators like $(3z^2 - r^2)/r^5$. As the expected value of this kind of orbital operator for an A_{1g} state is zero it turns out that the A parameter should be equal to zero. However, this fact is contrary to experimental findings for Mn^{2+} and Fe^{3+} impurities derived through EPR and Mössbauer spectroscopies [139, 164]. This puzzling fact reflects the polarization of

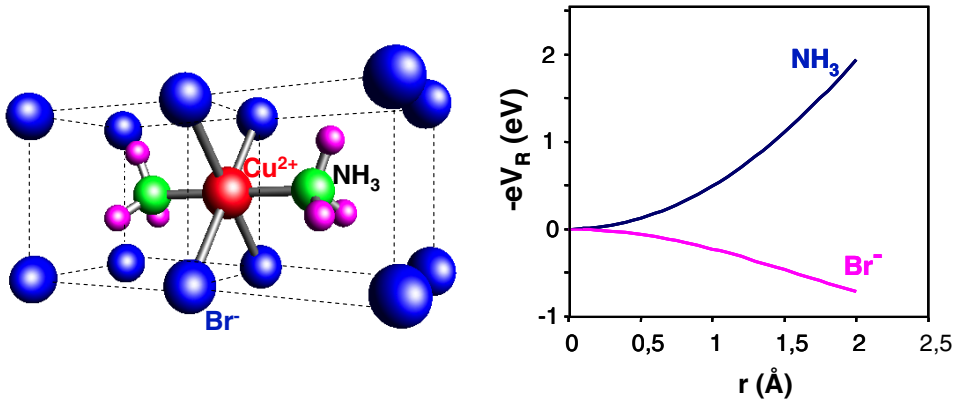

Figure 3. Left: description of the substitutional $CuBr_4(NH_3)^{2-}$ complex formed inside the NH_4Br lattice. Cu^{2+} does not replace the host lattice cation but it is located interstitially. Right: picture of the $V_R(\mathbf{r})$ potential for the $CuBr_4(NH_3)^{2-}$ complex embedded in NH_4Br. The origin is taken at the Cu^{2+} ion. Results are shown for $\mathbf{r}$ along Cu–Br and Cu–N directions.

inner 1s, 2s and 3s shells of cations due to the exchange interaction with unpaired valence electrons. If there is an unpaired electron with spin up in the open shell, the wavefunction of 1s electrons with spin up is not the same as that for electrons with spin down. In comparison to the 1s↓ electron the 1s↑ one can be closer to 3d↑ as the latter electron will never be at the same point *simultaneously*. This fact thus implies a negative spin polarization on the nuclei and then a non-zero contribution of the isotropic Fermi contact interaction [139].

Polarization of closed shells can play an important role in understanding the superhyperfine tensor in cases where the contribution coming from the simple bonding description (3) is zero. This happens, for instance, for d^9 ions in an elongated octahedral geometry with an unpaired electron in the $x^2 - y^2$ orbital. Although any admixture with p and s valence orbitals of *axial* ligands is symmetry forbidden the corresponding superhyperfine interaction has sometimes been detected through EPR [165].

For d impurities with $S > 1/2$ the zero-field splitting term, H_{ZFS}, has to be included into the spin Hamiltonian (4) when the local symmetry changes from O_h to D_{4h} [139, 141]:

$$H_{ZFS} = D(S_z^2 - S^2/3). \tag{7}$$

This term reflects the partial raising of the degeneracy compatible with the symmetry and the Kramers theorem.

2.3. Influence of the rest of the ions in the lattice upon the complex

Although very often active electrons coming from a transition-metal impurity M are *confined* in the MX_N complex this does not mean necessarily that its properties can be explained by considering *only* the complex *in vacuo*. In fact, the electrons of the MX_N complex also experience the electrostatic potential, V_R, arising from the rest of the ions in the lattice. However, it was first pointed out by Sugano and Shulman [82] that, for cubic crystals, V_R is almost (but not exactly) flat in the complex region and thus the influence of V_R for explaining the properties of TM impurities is usually ignored. Nevertheless, it has been pointed out that V_R can play an important role not only when the local symmetry is lower than cubic but also in understanding the different properties displayed by the same impurity embedded in two non-isomorphous lattices [166]. Let us first consider the $CuX_4(NH_3)_2^{2-}$ centre (X = Cl, Br) formed in lattices like NH_4Cl, CsCl or NH_4Br (figure 3(a)) [43–47]. Although the host lattice

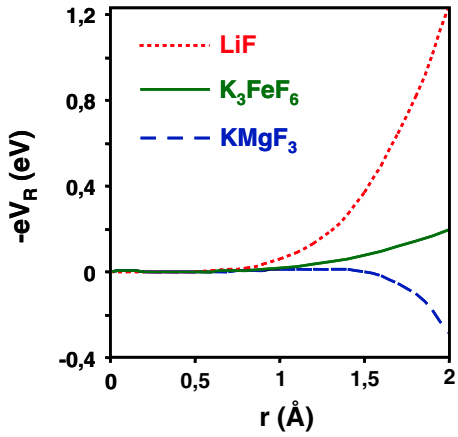

Figure 4. Representation of the electrostatic potential due to the rest of the lattice, V_R, on the FeF_6^{3-} complex embedded in LiF, K_3FeF_6 and $KMgF_3$, along a metal–ligand direction.

is cubic the Cu^{2+} impurity is not substitutional but occupies an interstitial position and thus the local symmetry around Cu^{2+} is tetragonal. The influence of V_R on electrons lying in the $CuX_4(NH_3)_2^{2-}$ complex [47] is depicted in figure 3(b) through the quantity $(-e)V_R$ (**r**) (e = proton charge). For this kind of complex V_R is flat just around $\mathbf{r} = 0$ due to the existence of inversion symmetry. However, when the electron is far from the origin (where the impurity is placed) significant deviations from flatness are exhibited by the V_R function. As shown in figure 3(b), V_R raises the levels coming from NH_3 ligands while it depresses those from X^- ones.

The electrostatic potential arising from the rest of the ions in the lattice can even be important for impurities in a true local cubic symmetry [30, 166]. In these cases V_R can lead to subtle differences when the properties generated by the same impurity in two *non-isomorphous* lattices are compared. For the sake of clarity let us consider an octahedral MX_6 complex embedded in cubic lattices like perovskites, alkali halides with NaCl structure or elpasolites. The form of V_R along a metal–ligand direction [30] for these three types of cubic lattice is displayed in figure 4. For a perovskite lattice $(-e)V_R(\mathbf{r})$ induces an energy decrement when the electron is close to a ligand and thus this energy lessening should be more important for a σe_g orbital than for a t_{2g} orbital which has a π character. By contrast, in the case of alkali halide or elpasolite structures, $(-e)V_R(\mathbf{r})$ induces (figure 4) an increase of the energy of e_g and t_{2g} levels. Therefore, if the influence of $V_R(\mathbf{r})$ is more significant on the e_g orbital than on the t_{2g} one it can be expected that $V_R(\mathbf{r})$ leads to a *supplementary* increase of $10Dq$.

Examples showing the key role played by V_R for explaining the properties of complexes in low lattice symmetry lattices are given in sections 4 and 5.

2.4. Elastic coupling of the complex with neighbour ions of the rest of the lattice

Even if valence electrons coming from an impurity M are confined within an MX_N complex, equilibrium distances and vibrational properties cannot in general be understood through the complex *in vacuo* [167, 168]. This means that elastic interactions of ligands with neighbour ions of the rest of the lattice are important as regards the frequencies of local or resonant modes which are often observed in low-temperature optical spectra [169, 21–25]. A simple model [168] for describing the elastic coupling of a complex with neighbour ions of the rest of

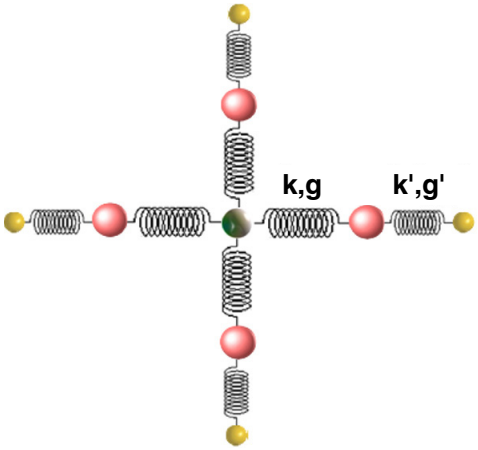

Figure 5. Model representing the elastic metal–ligand and ligand–next-neighbour bonds connected by springs with parameters (k, g) and (k', g'), respectively. k and k' are force constants while g and g' describe the anharmonicity as detailed in equation (47).

the lattice is depicted in figure 5. The constant k describes the interaction between the impurity and ligands of the MX_N complex in the harmonic approximation while k' simply depicts the interaction of ligands with neighbour ions of the rest of the lattice. When the nominal charge of the impurity is higher than that of the substituted lattice ion, the elastic decoupling with the rest of the lattice is favoured. This situation has been well verified in the case of *divalent* impurities in alkali halide lattices where it is found that $k \gg k'$ [94, 33]. In these cases, the equilibrium impurity–ligand distances are only slightly dependent upon the host lattice. For instance, it has been found [84] that on passing from KCl ($R_H = 3.14$ Å) to RbCl ($R_H = 3.29$ Å) the distance, R, between the Tl^{2+} impurity and Cl^- ligands increases only by 0.02 Å. In other words, the f quantity

$$f = \Delta R/\Delta R_H \tag{8}$$

is equal only to ∼0.1. A similar situation can be encountered in an elpasolite host lattice [26] where adjacent trivalent ions do not have any common ligand [170]. The degree of elastic coupling increases for cubic fluoroperovskites like $KMgF_3$ doped with divalent cations such as Mn^{2+} or Ni^{2+} (where $f \approx 0.3$) [132, 18–20] while for Cu^{2+}-doped cubic oxides like MgO, CaO and SrO the impurity–ligand distance is determined mainly by the host lattice ($f \approx 0.7$) [171].

In principle an impurity modifies the position of ions other than nearest neighbours. Nevertheless in a *three-dimensional* compound the components of the strain generated by the impurity depend on R_I^{-3}, where R_I stands for the distance between an ion and the impurity [172]. When $|(R/R_H) - 1| \approx 5\%$ it is thus not unreasonable to assume that other ions outside the complex keep their host lattice positions [19]. However, in cases like KCl:Ag^0 where $|(R/R_H) - 1| = 20\%$ second neighbours along ⟨100⟩ directions are found to experience a significant relaxation as well [135].

3. Pressure influence on spectroscopic parameters of model systems

3.1. Relevant experimental data

3.1.1. Optical data. Since the early work by Drickamer [101], it is known that Racah parameters B and C are, in general, less sensitive to the influence of an applied hydrostatic

pressure than $10Dq$ [173–175]. The first measurements carried out on the cubic charge transfer insulator NiO [176] showed that the dependence on the metal–ligand distance at different hydrostatic pressures can be written as

$$10Dq = K R^{-n}. \tag{9}$$

For NiO a value $n = 5$ was found [176]. A similar law was derived for ruby with an exponent $n = 4.5$ obtained assuming that the local compressibility around Cr^{3+} is the same as for pure Al_2O_3 [173, 175]. Values of the exponent n close to 5 have also been found in the cubic compound NH_4MnCl_3 [177] and for other cubic systems like $K_2NaGaF_6{:}Cr^{3+}$ [178], $Cs_2NaYCl_6{:}Cr^{3+}$ [179] explored through different applied hydrostatic pressures.

The effects of changing the host lattice embedding the MX_6 complex upon both $10Dq$ and R has also been investigated. As an example, the CF spectra of $RbMnF_3$, $KMnF_3$, $KMF_3{:}Mn^{2+}$ (M = Mg, Zn), $RbCaF_3{:}Mn^{2+}$, $RbCdF_3{:}Mn^{2+}$ and $CsCaF_3{:}Mn^{2+}$ have been explored through optical spectroscopy [18, 180]. In the case of doped systems the information was derived from the excitation spectra of the only luminescent channel $^4T_{1g} \rightarrow {}^6A_{1g}$. For these systems B and C parameters have been found to vary slightly along the series of compounds, while $10Dq$ is quite sensitive to the chemical pressure, the exponent n being equal to 4.7 [180]. This figure is quite comparable to those found by applying a hydrostatic pressure on a given system and thus stresses that the $10Dq$ value is originated inside the MnF_6^{4-} complex indeed. Recently, the properties of $KMgF_3{:}Mn^{2+}$ and $RbCdF_3{:}Mn^{2+}$ have been studied by means of density functional theory (DFT) based calculations performed at different values of the lattice parameter a [181]. Through this kind of *ab initio* calculation it is thus possible to simulate the effects of pressures (positive and also negative) on both systems. As a salient feature, when pressure induces the same R value for both $KMgF_3{:}Mn^{2+}$ and $RbCdF_3{:}Mn^{2+}$ the calculated value of $10Dq$ is found to be the same for such systems. On the other hand, the equilibrium R values for different fluoroperovskites doped with Mn^{2+} are found to be *ordered*, following the a parameter of the host lattice [181, 19].

The different sensitivity of Racah parameters and $10Dq$ to R changes can be well seen looking at CrO_6^{9-} complexes formed in oxides where $10Dq$ values are in the range 16 000–18 000 cm^{-1} [10, 173, 175]. Therefore, as the energy, E, of the $^4A_{2g}(t_{2g}^3) \rightarrow {}^4T_{2g}(t_{2g}^2 e_g)$ transition is just equal to $10Dq$ [83] it can be expected that $dE/dR \approx 400\ cm^{-1}\ pm^{-1}$. This can be compared with the value $dE/dR = 7\ cm^{-1}\ pm^{-1}$ derived for the $^2E_g(t_{2g}^3) \rightarrow {}^4A_{2g}(t_{2g}^3)$ sharp transition in ruby [173, 182].

It is worth noting that this huge difference in sensitivity to pressure has important consequences as regards the *shape* of bands related to both transitions. In fact, the Huang–Rhys factor, S_a, reflecting the coupling of the excited state with the symmetric a_{1g} mode, is proportional to $(dE/dR)^2$ [183, 179, 175]. For CrF_6^{3-} complexes in cubic fluorides the Huang–Rhys factors for the excited $^4T_{2g}(t_{2g}^2 e_g)$ state corresponding to a_{1g} and e_g modes both lie between 1 and 2 [63, 183]. Therefore, vibrational progressions involving both modes can be observed in the low-temperature optical spectra [21–25]. By contrast, if S_a for the $^2E_g(t_{2g}^3)$ state is expected to be $\sim 4 \times 10^{-4}$ then no vibrational replica should in practice be observed, thus leading to a sharp $^2E_g(t_{2g}^3) \rightarrow {}^4A_{2g}(t_{2g}^3)$ band. Additional discussion on this matter is given in section 7.

The $10Dq$ parameter can be used for monitoring the R changes induced by an applied hydrostatic pressure on a doped lattice. It can also be employed for measuring the effects of different chemical pressures on the impurity–ligand distance [180, 18]. In the latter case this procedure can rigorously be applied *only* if all host lattices where the MX_N complex is inserted are isomorphous. Further discussion on this issue is provided in section 4.

Table 2. Experimental A_s and A_{an} values (in MHz) measured for Ni^{2+} in several cubic fluoroperovskites. The values of the estimated Ni^{2+}–F^- distance, R, and the corresponding for the perfect lattice, R_H, are also given. Data are taken from [20].

Lattice	R_H (Å)	R (Å)	A_s	A_{an}
$KMgF_3$	1.987	1.99	117.6	30.3
$CsCdF_3$	2.263	2.05	93.6	27.9
$CsCaF_3$	2.281	2.06	90.3	28.5

Experimental information on dE/dR values for CT transitions of model systems is scarcer than for crystal field excitations. No measurement of a CT transition related to a 3d impurity in pure octahedral symmetry under a hydrostatic pressure has been reported up to now. Nevertheless, the influence of the chemical pressure upon the allowed CT transitions can be well seen in the magnetic circular dichroism data obtained for Tl^{2+} impurities ($6s^1$ configuration) in several alkali halides [184]. For instance, on passing from KCl to RbCl the first allowed CT undergoes a red shift of 1200 cm^{-1}. As R is calculated to increase by 2 pm [84] on passing from KCl:Tl^{2+} to RbCl:Tl^{2+} this means a value $dE/dR \approx -600$ cm^{-1} pm^{-1}. Similar values were found for compounds involving square-planar $CuCl_4^{2-}$ units [84].

The significant sensitivity of CT transitions to R changes is also supported by the blue shift experienced upon cooling in the case of divalent 3d ions in alkali chlorides and bromides [142, 143]. Assuming that such a blue shift is mainly due to thermal expansion effects, values of dE/dR between -500 and -1000 cm^{-1} pm^{-1} are derived. Calculated values of CT transitions [84] for different complexes underline that, in general, this kind of transition does depend more strongly on R than CF ones. This trend is also consistent with the bigger bandwidths of CT transitions in comparison to those displayed by CF excitations.

3.1.2. Hyperfine constants for octahedral complexes with σ bonding in the ground state. For octahedral centres of Mn^{2+} or Fe^{3+} impurities in halide lattices, the ground state usually corresponds to the high-spin configuration $^6A_1(t_{2g}^3e_g^2)$ [139]. Thus, in these cases as well as for Ni^{2+} impurities in a similar situation (ground state $^3A_2(t_{2g}^6e_g^2)$), there are also unpaired electrons in the antibonding e_g level with σ bonding. Unpaired e_g electrons can be present in the ground state of Mn^{3+} ($t_{2g}^3e_g^1$ configuration), Rh^{2+}($t_{2g}^6e_g^1$ configuration) or Cu^{2+}($t_{2g}^6e_g^3$ configuration). In all these cases the JT instability favours however a non-cubic equilibrium geometry. This point is discussed in section 5.

The Ni^{2+} impurity in several cubic fluorides has been investigated by means of EPR and ENDOR spectroscopy [16, 20, 139, 185]. Measured values of the two superhyperfine constants, A_{an} and A_s, for doped cubic fluoroperovskites are gathered in table 2. It can be noticed that while the reported A_{an} value is practically the same for all systems the A_s value for $KMgF_3$:Ni^{2+} is about 30% higher than that for $CsCaF_3$:Ni^{2+}. A similar situation is found when dealing with O_h MnF_6^{4-} or FeF_6^{3-} units in cubic lattices [17, 29, 30] and also for elongated NiF_6^{5-} complexes or square-planar NiF_4^{3-} units where the unpaired electron lies in a $b_{1g} \sim x^2 - y^2$ orbital [165]. The results of table 2 strongly suggest that A_s is much more sensitive than A_{an} to R variations induced by the chemical pressure. As for NiF_6^{4-} the anisotropic constant, A_{an}, is related to λ_σ^2, this fact suggests that λ_s^2 strongly depends on R but not λ_σ^2. This conclusion is certainly surprising as the covalency is dominated by the transfer of the e_g unpaired electrons from nickel to $2p_\sigma$ orbitals of fluorine ligands. More precisely, from the analysis of A_{an} and A_s parameters there is found [20] a ratio $\lambda_\sigma^2/\lambda_s^2 \approx 6$ for NiF_6^{4-} in cubic fluoroperovskites.

The experimental A_s parameter has been used for measuring the variations of R produced by the action of different cubic lattices upon octahedral NiF_6^{4-}, MnF_6^{4-} and FeF_6^{3-} complexes [132, 20, 30]. Writing

$$A_s = CR^{-n_s}, \tag{10}$$

values of the n_s exponent in the range 6.5–8 have been encountered. For NiF_6^{4-} complexes in fluoroperovskites (table 2) $n_s = 7.6$, implying $dA_s/dR = -3.5$ MHz pm^{-1}.

Alternatively the dependence of A_s on R has been modelled [132] by considering that it is proportional to the λ_s^2 coefficient defined in equation (3), while λ_s is just given by

$$\lambda_s = cS_s; \qquad S_s = \langle d, \Gamma | \chi_s, \Gamma \rangle \tag{11}$$

where $c \geqslant 1$ is a constant and S_s is a group overlap integral involving the valence s orbitals of ligands. The analysis through equation (11) of the experimental A_s value for Ag^0- and Cu^0-doped alkali halides has provided strong evidence of a huge relaxation of ligands [186, 134, 135].

EPR data on Mn^{2+}-doped cubic fluoroperovskites reveal that, within experimental uncertainties, the measured hyperfine constant, A, is the *same* and equal to -273 ± 3 MHz [17]. This is quite reasonable bearing in mind that A comes from the spin polarization of inner 1s, 2s and 3s shells [139]. Careful ENDOR measurements of A carried out on $CsCaF_3$:Mn^{2+} ($A = -276.7$ MHz) [187] and MgF_2:Mn^{2+} ($A = -274.2$ MHz) [188] suggest that $dA/dR \approx -0.4$ MHz pm^{-1}. This figure, also obtained through calculations on MnF_6^{4-} [166], underlines that $A^{-1}(dA/dR)$ is two orders of magnitude smaller than $A_s^{-1}(dA_s/dR)$.

3.2. Microscopic insight

This section is addressed to gaining a better insight into the origin of main facts described in section 3.1 with the help of calculations and physical models.

3.2.1. Charge transfer transitions. Let us now mention the results of theoretical calculations carried out on octahedral MX_6 (X = F, Cl, Br) complexes [26, 84, 147, 189] and tetrahedral units like FeO_4^{2-} or CrO_4^{4-} [190–194]. Typically, they lead to values of dE/dR in the range between -500 and -1500 cm^{-1} pm^{-1} for allowed CT transitions involving d levels with σ character. So, for the first CT transition there are calculated values $dE/dR \approx -1600$, -900 and -530 cm^{-1} pm^{-1} for CrF_6^{3-}, CrO_4^{4-} and $TlCl_6^{4-}$, respectively [84, 147, 189, 192]. Also for the CT transitions of the square-planar $CuCl_4^{2-}$ unit the corresponding dE/dR value for the first allowed CT transition $e_u \rightarrow b_{1g}(x^2 - y^2)$ is found to be equal to -600 cm^{-1} pm^{-1} [84]. It is worth noting that in the case of CrF_6^{3-} complexes a value $dE/dR \approx -1100$ cm^{-1} pm^{-1} has been found for the $t_{1u} \rightarrow t_{2g}$ transition, where $t_{2g}(xy, xz, yz)$ has a π character. Then, this quantity is again negative but its absolute value is, as expected, smaller than $|dE/dR| \approx 1600$ cm^{-1} pm^{-1} found for the $t_{1u} \rightarrow e_g(x^2 - y^2, 3z^2 - r^2)$ transition [147].

Aside from confirming the strong sensitivity of CT maxima to R variations these data suggest that dE/dR is *negative* for octahedral and tetrahedral complexes. This fact means that the CT energy of an octahedral complex should experience a blue shift under an applied hydrostatic pressure. In other words, as the bulk modulus is always positive then

$$(\partial E/\partial p)_T > 0 \tag{12}$$

for a CT transition corresponding to an octahedral complex.

It has been pointed out that all these facts are mainly due to the increase of electrostatic repulsion of ligands on electrons lying in the impurity when R decreases [84, 192]. For

clarifying this matter it is helpful to consider an *ionic* MX_6 complex in a cubic lattice. Equations (1) and (2) can then be written as

$$\begin{aligned}\varepsilon_M(d) &= -I_{0M} - eV_C = -I_{0M} - 6z_L e^2/R - eV_R \\ \varepsilon_L &= -I_{0L} - eV_A = -I_{0L} + (e^2/R)(-3.32\, z_L - z_M) - eV_R.\end{aligned} \tag{13}$$

Here z_L means the total charge on the ligand ion and V_R is the electrostatic potential due to all ions in the rest of the lattice *not* included in the complex. As for a cubic lattice V_R is very flat along the complex region, the sensitivity of $\varepsilon_M(d) - \varepsilon_L$ to R changes can be mainly due to terms involving $1/R$ in (9). Therefore, dE/dR can be approximated by

$$dE/dR \approx -(z_M - 2.68z_L)e^2/R^2. \tag{14}$$

Then, taking $z_M = 2, z_L = -1$ and $R = 2.2$ Å the simple equation (14) leads to $dE/dR = -1100\ \text{cm}^{-1}\ \text{pm}^{-1}$. Although this simple estimation explains the sign and the absolute values of dE/dR for CT transitions the situation becomes more complex as the covalency increases. This circumstance is favoured by an increase of the nominal charge of the impurity ion. There are three factors favouring a reduction of dE/dR with respect to the value expected for a pure ionic situation when the covalency increases progressively [192]: (i) the values of $|z_L|$ and especially z_M are lessened; (ii) I_{0M} and I_{0L} in equation (13) should now be understood to depend on the actual value of z_M and z_L charges which can be non-integer; (iii) when the electron jumps to an antibonding level it also spends some time on ligands.

For an ionic complex one would expect that a CT transition leads to a transfer of an electron from ligands to the impurity cation. However, calculations reveal that the total charge, z_M, on the impurity in the CT state can be quite close to that of the ground state [195, 194, 192, 26]. This important phenomenon cannot be understood considering that one-electron orbitals are unmodified after the CT jump. In fact, once a hole is created on a ligand orbital there is a significant relaxation of electronic orbitals inducing a net flow of the electronic charge from metal to ligands. This effect increases the value of z_M and I_{0M}, thus lessening the energy of the CT state. The electronic relaxation is accomplished by an increase of the electronic density on the metal for antibonding levels as well as by the corresponding reduction for *filled* bonding orbitals. A more detailed discussion on this matter can be found in [84].

3.2.2. Unpaired spin densities and superhyperfine constants. Different calculations performed for octahedral complexes like NiF_6^{4-}, MnF_6^{4-} or FeF_6^{3-} have found that [83, 196–199, 30]: (i) the electronic charge, $\sim\lambda_\sigma^2$, transferred to $2p_\sigma$ orbitals of F^- ligands in the antibonding e_g level, is much higher than λ_s^2 describing the corresponding electronic charge on 2s orbitals; (ii) λ_s^2 is found to be much more sensitive than λ_σ^2 to R variations and the calculated R dependence of λ_s^2 is consistent with the n_s exponent derived from experimental A_s values lying typically between 6 and 8.5.

Although these conclusions concur with the analysis of experimental superhyperfine constants given in section 3.1.1 it is however necessary to understand the main origin of these relevant facts [200, 84].

As depicted in equation (3), chemical bonding in a MX_6 complex produces an admixture of a $|d, \Gamma\rangle$ metal wavefunction with the corresponding $|\chi_p, \Gamma\rangle$ and $|\chi_s, \Gamma\rangle$ ligand wavefunctions. In the traditional molecular orbital picture this admixture arises from the off-diagonal matrix elements $\langle d,\ \Gamma|h|\chi_p, \Gamma\rangle$ and $\langle d,\ \Gamma|h|\chi_s, \Gamma\rangle$ involving the one-electron Hamiltonian, h [83, 201]. For an MX_6 complex with high ionic character λ_σ can thus be approximated by

$$\lambda_\sigma = \frac{\langle d, \Gamma|h|\chi_{p\sigma}\rangle}{\varepsilon_M(d) - \varepsilon_L(p)}. \tag{15}$$

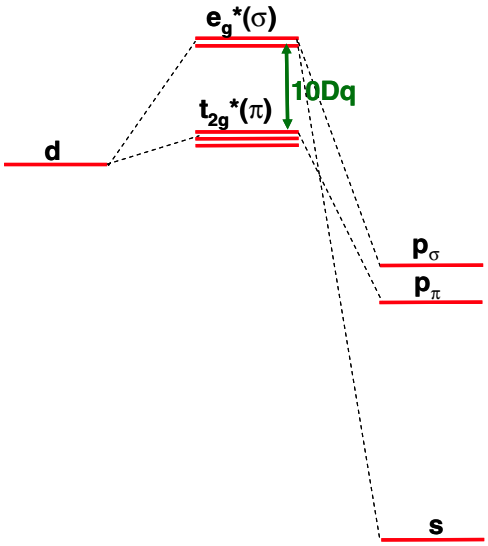

Figure 6. Molecular orbital diagram showing the interactions between metal and p and s ligand orbitals responsible for the cubic field splitting energy, $10Dq$, in an octahedral MX_N complex.

Here $\varepsilon_M(d)$ and $\varepsilon_L(p)$ are the one-electron energies of the impurity d level and the p valence orbital of a ligand, respectively. Assuming now that the R dependence of $\langle d, \Gamma|h|\chi_{p\sigma}, \Gamma\rangle$ roughly follows that of the group overlap integral

$$S_{p\sigma} = \langle d, \Gamma|\chi_{p\sigma}, \Gamma\rangle, \tag{16}$$

then the absolute value of the numerator in equation (15) does increase when the MX_6 complex is squeezed. However, the denominator, $\varepsilon_M(d) - \varepsilon_L(p)$, in equation (15) essentially means a CT excitation and thus, according to results of the preceding section, it *also* increases when R decreases. The substantial cancellation of the increase of $S_{p\sigma}$ by that of $\varepsilon_M(d) - \varepsilon_L(p)$ is thus responsible for the slight dependence of λ_σ^2 on R [200]. This fact is also relevant because as $\lambda_\sigma^2 \gg \lambda_s^2$ it also suggests that N_e^2 in (3) and the total charge, z_M, on the central atom are slightly dependent on R.

The quite different behaviour displayed by λ_s^2 and λ_σ^2 parameters is ultimately related to the big separation between valence s and p levels of common ligands like halide ions or O^{2-} [132, 200]. It is well known that the separation between such levels is strictly zero if the central field potential is Coulombian [202]. For this reason the s–p separation increases progressively along a row of the periodic table. So the 2s–2p separation is equal to 1.9 eV for Li and 4.5 eV for carbon, while at the end of the series it reaches a value close to 17 eV for oxygen and around 23 eV for both the fluorine atom and F^- ion [130, 84]. Owing to this relevant fact, the 2s level can play an equivalent role to that of 2p orbitals in the chemical bonding of elements like Li, Be or C but *never* when fluorine or oxygen are involved, where the 2s admixture should have a *perturbative* character.

Bearing in mind figure 6, similarly to equation (11) there can be written for λ_s

$$\lambda_s = \frac{\langle d, \Gamma|h|\chi_{s\sigma}\rangle}{\varepsilon_M(d) - \varepsilon_L(s)}. \tag{17}$$

Because of the big separation between the d levels of the impurity and the s valence orbital of the ligand ion, in this case the *relative* variation of the $\varepsilon_M(d) - \varepsilon_L(s)$ quantity is certainly

Table 3. Calculated values of $10Dq$ (in cm^{-1}) for CrF_6^{3-} at two different distances (in pm) through a normal calculation and another one where the 2s(F) orbitals are removed from the basis set. First (second) row values (taken from [93]) have been obtained by the self-consistent charge extended Hückel (MSX α) method.

R	$10Dq$ (normal)	$10Dq$ (calculation without 2s)
185	18 538	3600
	18 800	6025
195	13 782	3917
	14 920	7238

much smaller than that of $\varepsilon_M(d) - \varepsilon_L(p)$ and it can thus be considered as a constant in the $\Delta R \sim 10$ pm interval. On the other hand, the overlap integral S_s varies more strongly with R than $S_{p\sigma}$ following the more internal character of the valence s orbital when compared to the corresponding p orbital. Both reasons are thus responsible for the high sensitivity of A_s to R variations, and they also explain why $\lambda_\sigma^2 \gg \lambda_s^2$ for octahedral MX_6 complexes with halides or O^{2-} as ligands [84].

3.2.3. Crystal field transitions: the dependence of 10Dq upon R. Even recently the R dependence of $10Dq$ observed experimentally for octahedral MX_6 complexes has been explained on the basis of the CF theory [23, 25]. In this framework, $10Dq$ is given by [83]

$$10Dq = \frac{5}{3}\frac{|z_L|e^2\langle r^4\rangle_d}{R^5}. \tag{18}$$

This expression is consistent with an R^{-5} dependence of $10Dq$, but it *also* leads to values of the cubic field splitting which may be one order of magnitude smaller than experimental ones [18, 84]. The pioneering work by Sugano and Shulman [82] on the octahedral NiF_6^{4-} unit already demonstrated that the $10Dq$ splitting mainly arises from the *different* chemical bonding in the antibonding e_g and t_{2g} levels of a properly considered MX_6 complex. It is worth noting that in this case σ bonding is present in e_g while not in the t_{2g} level which only exhibits π bonding (figure 6).

Calculations performed treating the d and ligand levels *on the same footing* have been able to reproduce the main features observed experimentally for CF spectra of MX_6 molecules embedded in insulating lattices. So, since the first work by Burns and Axe [203] it was noted that theoretical calculations of MX_6 complexes lead to reasonable values of *both* $10Dq$ and the exponent n defined in equation (6). The value of this exponent was found to lie typically in the range 3.5–6 [204–207, 183, 167, 26].

The use of different basis sets has shed light on the origin of the R dependence of $10Dq$ [93, 208]. For the sake of clarity let us now consider the CrF_6^{3-} complex. In a first step normal calculations have been carried out where both 2p and 2s orbitals of fluorine are included in the basis set. However, in a second step the 2s(F) orbitals have been suppressed from it. This process can be performed using the extended Hückel and MSX α methods where the suppression of orbitals from the basis set can easily be done. The comparison of $10Dq$ values obtained by the two procedures is given in table 3. It can be noticed that while in the normal calculation $10Dq$ is found to increase significantly on passing from $R = 195$ to 185 pm (involving an exponent n close to 5), dramatic changes are however found when the 2s(F) orbitals are removed. In fact, under this suppression $10Dq$ is found to remain constant or even increase slightly when R does while the $10Dq$ value itself is found to experience a significant decrement. Similar results to those gathered in table 3 have been obtained for other octahedral

or tetrahedral complexes involving halides or oxygen as ligands. All these facts stress the key role played by the *small* 2s(F) admixture in the antibonding e_g orbital (figure 1) as regards the R dependence of $10Dq$ [93, 208]. This conclusion is somewhat surprising because, for complexes like CrF_6^{3-}, MnF_6^{4-} or NiF_6^{4-}, λ_s^2 lies typically between 2% and 4% [83, 196, 93, 30]. However, this puzzling situation can be rationalized by considering the mechanisms behind the splitting between e_g and t_{2g} levels. As shown in figure 6, a $|d, e_g\rangle$ orbital interacts through the one-electron Hamiltonian, h, with two different linear combinations, $|\chi_p, e_g\rangle$ and $|\chi_s, e_g\rangle$, with σ character. This interaction is also responsible for the λ_σ and λ_s admixture coefficients (as shown in equations (12) and (14)) and produces in second-order perturbation an energy raising of the antibonding e_g level. By contrast, symmetry avoids any linear combination $|\chi_s, t_{2g}\rangle$ and thus the $|d, t_{2g}\rangle$ orbital can only interact with a $|\chi_p, t_{2g}\rangle$ linear combination with π character, leading also to an increase of the t_{2g} energy level. Bearing in mind these facts and equations (15) and (17), the values of $10Dq$ for a complex with dominant ionic character can be approximated by [208, 84, 93]

$$10Dq \cong (\varepsilon_M(d) - \varepsilon_L(p))\{\lambda_{p\sigma}^2 - \lambda_{p\pi}^2\} + (\varepsilon_M(d) - \varepsilon_L(s))\,\lambda_s^2. \tag{19}$$

This simple equation underlines that the influence of the 2s(F) admixture upon $10Dq$ can be comparable to that derived from the 3d–2p hybridization for both e_g and t_{2g} levels. In fact, if $\varepsilon_M(d) - \varepsilon_L(p)$ is around 7 eV for a MF_6 complex it can be expected that $\varepsilon_M(d) - \varepsilon_L(s) \approx 30$ eV. On the other hand, equation (16) stresses that the R dependence of $10Dq$ is ultimately related to that of λ_s^2 which has been discussed in sections 3.1.1 and 3.2.2. Theoretical calculations like those carried out on MnF_6^{4-} complexes reproduce the small dependence of the Racah parameters, B and C, upon R [167, 198, 209]. This situation can roughly be understood considering that in the case of a complex such parameters are determined by the time spent by electrons of non-filled shells on the central ion [210]. In other words, a Coulomb integral like $\langle e_g(1)e_g(2)|e^2/r_{12}|e_g(1)e_g(2)\rangle$ can be well approximated by

$$\langle e_g(1)e_g(2)|e^2/r_{12}|e_g(1)e_g(2)\rangle \simeq N_e^4\langle d(1)d(2)|e^2/r_{12}|d(1)d(2)\rangle. \tag{20}$$

Therefore, if N_e^2 is slightly dependent upon R (as discussed in section 3.2.2) this also roughly explains the slight sensitivity of B and C to changes in R.

4. Transferability of laws to lower symmetry systems

It is now crucial to discuss whether the laws obtained for octahedral MX_6 complexes in cubic lattices can or cannot be transferred to lower symmetry complexes which besides can be embedded in a lattice which is non-cubic. It will be shown that the information derived from spectroscopic parameters of low-symmetry systems using the laws described in section 3 can lead, in general, to wrong conclusions. Two reasons are behind this discrepancy: (i) the symmetry change undergone by the MX_N complex which can modify the *nature* of orbitals of unpaired electrons; (ii) the existence of electric fields inside the MX_N complex arising from the ions of the rest of the lattice.

4.1. Modifications from the symmetry lowering of the complex

For the sake of clarity only complexes with D_{4h} or C_{4v} symmetry will be analysed in this section. In particular, the isotropic superhyperfine constant of MX_4 square-planar units and tetragonal MX_6 complexes ($M = d^9$ and d^7 ions) will first be considered. For an MX_6 complex with D_{4h} symmetry there are two metal–ligand distances, namely the equatorial, R_{eq}, and the axial, R_{ax}. Thus, tetragonal MX_6 complexes can be elongated ($R_{eq} < R_{ax}$) or compressed

($R_{eq} > R_{ax}$). In the analysed MX_4 complexes and *elongated* MX_6 complexes of d^9 ions the unpaired electron lies in the $b_{1g} \sim x^2 - y^2$ orbital, while for the compressed ones and elongated MX_6 complexes of d^7 ions it is in the $a_{1g} \sim 3z^2 - r^2$ orbital.

4.1.1. Changes in isotropic superhyperfine and hyperfine constants. Theoretical calculations have been performed for a variety of MX_4 and MX_6 complexes of d^9 ions at different values of the R_{eq} distance [200, 211, 212]. From them, the dependence of λ_s^2 upon R_{eq} has been explored. It turns out that huge differences are found when comparing elongated and square-planar units with compressed complexes [211]. Writing, similarly to (10),

$$\lambda_s^2(\text{eq}) \propto R_{eq}^{-n_s}, \tag{21}$$

the values of the exponent n_s for elongated and square-planar units are found to lie in the range 6–8 and they are thus quite comparable with those derived for octahedral MX_6 complexes. For this reason, the superhyperfine $A_s(\text{eq})$ constants of elongated NiF_6^{5-} and square-planar NiF_4^{3-} complexes placed in different lattices have been used for deriving information about R_{eq} [200, 165]. By contrast, the exponent n_s calculated for a compressed CuF_6^{4-} complex is found to be equal only to 2, while for $CuCl_4NH_3^{2-}$ $n_s = 1.5$ [211]. The reason for this relevant difference has been ascribed to the change undergone by the nature of the HOMO orbital on passing from O_h to D_{4h} symmetry in the case of the compressed complex. In this case, the *form* of the $3z^2 - r^2$ orbital is no longer that described by equation (3) for an octahedral symmetry because the hybridization with the 4s orbital of Cu^{2+} is now allowed [211]. By contrast, any admixture of 4s or 4p orbitals into $x^2 - y^2$ is forbidden in D_{4h} symmetry.

The study of the d^7 centre Rh^{2+}-doped NaCl has shown the importance of the 4d–5s hybridization for understanding the superhyperfine constants in D_{4h} symmetry. Although in O_h symmetry the $RhCl_6^{4-}$ complex would have a $t_{2g}^6 e_g^1$ configuration, it does however exhibit an elongated geometry, the unpaired electron being thus in a $\sim 3z^2 - r^2$ orbital [213, 32]. As this orbital has bonding with *both* axial and equatorial ligands, the corresponding superhyperfine constants $A_s(\text{ax})$ and $A_s(\text{eq})$ have been calculated [33] as a function of the $\eta > 0$ parameter defined by

$$R_{ax} = R_{OC} + 2\eta; \qquad R_{eq} = R_{OC} - \eta \tag{22}$$

where R_{OC} stands for the equilibrium Rh^{2+}–Cl^- distance *imposing* an O_h symmetry. Surprisingly, it is found that when R_{eq} is reduced $A_s(\text{eq})$ also decreases, while the ratio $A_s(\text{ax})/A_s(\text{eq})$ increases slightly. These puzzling facts can reasonably be accounted for by considering the effect of the 4d–5s hybridization upon $A_s(\text{ax})$ and $A_s(\text{eq})$ [33]. The hybrid wavefunction is briefly depicted by

$$|3z^2 - r^2\rangle + \varepsilon|(n+1)s\rangle. \tag{23}$$

Therefore if $R_{ax} > R_{eq}(\eta > 0)$ the repulsion of ligands upon the unpaired electron can be lowered, enhancing the electronic density along the OZ axis while reducing that in the perpendicular XY plane. This implies $\varepsilon > 0$ for this situation which is qualitatively depicted in figure 7.

The importance of the nd–$(n+1)$s hybridization for modifying in a tetragonal symmetry the laws derived for O_h units can also be remarked when looking at the isotropic hyperfine constant of complexes with an unpaired electron in $3z^2 - r^2$ [213–215, 108, 44]. Let us first consider the $CuCl_4NH_3^{2-}$ centre formed in lattices like NH_4Cl or CsCl [43–45]. In addition to studies on this centre under different chemical pressures [215], EPR data on $CuCl_4ND_3^{2-}$ in ND_4Cl under hydrostatic pressure reveal that the hyperfine constants, $A_\parallel$ and $A_\perp$, are both positive and very sensitive to changes of metal–ligand distances [44]. These characteristics are

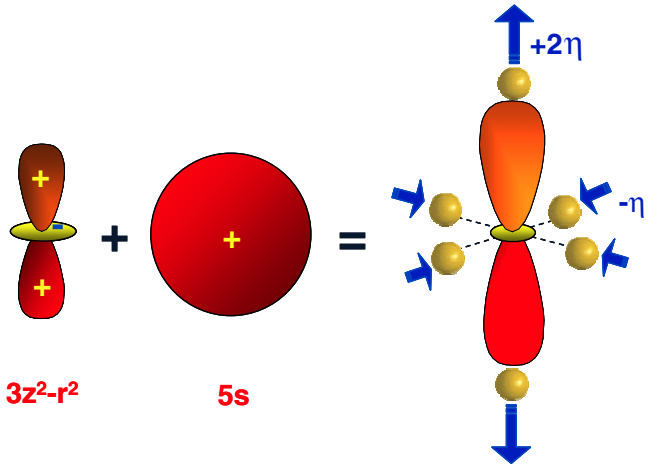

Figure 7. Schematic picture of electronic density changes induced by the $4d(3z^2 - r^2)$–5s hybridization in Rh^{2+}-doped NaCl.

thus quite different from the contribution of the polarization of inner shells [139] discussed in section 3.1.1 and they have been ascribed to the nd–$(n + 1)$s hybridization. Due to this mechanism the isotropic hyperfine constant, A_{iso}, can be approximated by

$$A_{iso} = -K + A_{(n+1)s}. \tag{24}$$

Here $K > 0$ reflects the contribution from inner shells, while $A_{(n+1)s}$ is proportional to ε^2 defined in equation (23). This confirms that $A_{iso} > 0$ values can be found by considering a hybridization as low as $\varepsilon^2 \approx 2\%$ [215]. Moreover, a big dependence of $A_{(n+1)s}$ upon both R_{eq} and R_{ax} is found through calculations. For the $CuCl_4NH_3^{2-}$ centre MSX α calculations lead to $dA_{iso}/dR_{ax} \approx 25$ MHz pm^{-1} [215], which has to be compared with the values $dK/dR = -0.4$ MHz pm^{-1} reported in section 3.1.1. The same idea embodied in equation (24) has been employed for explaining a null hyperfine tensor for $RhCl_6^{4-}$ in NaCl [216].

4.1.2. Changes in laws involving charge transfer transitions. It was concluded in section 3.2.1 that a CT transition of an octahedral MX_6 complex would experience a blue shift under a hydrostatic pressure. Nevertheless, experimental results on $(C_2H_5NH_3)_2CdCl_4$:Cu^{2+} show [217] that the *elongated* $CuCl_6^{4-}$ unit in such a compound undergoes a red shift when hydrostatic pressure is applied. This result points out again that conclusions reached for high-symmetry complexes in insulators can hardly be transferred to systems with a lower symmetry. For explaining this seemingly surprising result it is worth recalling here the basis leading to the conclusion embodied in equation (12). If the calculations on octahedral MX_6 complexes give $dE/dR < 0$ the conclusion $(\partial E/\partial p)_T > 0$ comes from the decrement of R induced *necessarily* by an increase of pressure. However, this statement is no longer true when the symmetry is reduced to D_{4h} and there are two different distances, R_{eq} and R_{ax}, in the complex. In this situation an applied hydrostatic pressure *necessarily* means a reduction of the volume of $CuCl_6^{4-}$ but not of *both* R_{eq} and R_{ax} distances. If $R_{ax} = 290$ pm and $R_{eq} = 230$ pm, the axial bond is softer than the equatorial one. Then, an applied pressure will reduce R_{ax} but can also lead to a slight increase of R_{eq} provided there is a lessening of the volume of the $CuCl_6^{4-}$ unit. In this situation a red shift of a CT transition can be observed if $|\partial E/\partial R_{eq}| \gg |\partial E/\partial R_{ax}|$. Detailed calculations on $CuCl_6^{4-}$ complexes support this view,

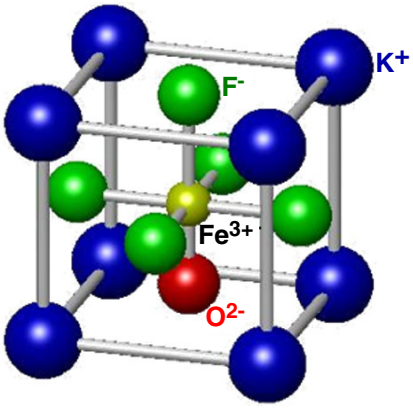

Figure 8. FeF_5O^{4-} complex embedded in the $KMgF_3$ lattice.

Table 4. A_s(eq) and A_s(ax) values (in MHz) measured for the $FeOF_5^{4-}$ in $KMgF_3$. Such values are compared with A_s for FeF_6^{3-} in two cubic fluoroperovskites. Data come from [68, 70] and [218].

Lattice	Centre	A_s(eq)	A_s(ax)
$KMgF_3$	$FeOF_5^{4-}$	72.3	30.8
	FeF_6^{3-}	71.2	71.2
$RbCdF_3$	FeF_6^{3-}	65.7	65.7

giving $\partial E/\partial R_{eq} = -256\ cm^{-1}\ pm^{-1}$ and $\partial E/\partial R_{ax} = -29\ cm^{-1}\ pm^{-1}$ [217]. These figures mean, in practice, that the energy of the first CT transition of the $CuCl_6^{4-}$ complex is only sensitive to variations of the equatorial distance. Therefore, the red shift observed for this complex in $(C_2H_5NH_3)_2CdCl_4$:Cu^{2+} under pressure likely reveals an increase of R_{eq} and a reduction of the tetragonality.

4.1.3. The $FeOF_5^{4-}$ centre in cubic fluorides: test of the superposition model. An interesting system in which to explore the transferability of laws from O_h to C_{4v} symmetry is the $FeOF_5^{4-}$ centre formed in cubic fluoroperovskites co-doped with both Fe^{3+} and O^{2-} impurities (figure 8) [68–70]. The local structure of this centre is determined once the two Fe^{3+}–F^- distances, R_{eq} and R_{ax}, and the Fe^{3+}–O^{2-} distance, called R_O, are known. Through EPR and ENDOR techniques the isotropic superhyperfine constants, A_s(ax) and A_s(eq), corresponding to the axial and four equatorial F^- ligands, respectively, of $FeOF_5^{4-}$ have been measured [68–70], and thus they can be compared with the A_s value for the O_h FeF_6^{3-} centre in the *same* lattice [218, 219, 29]. A_s(ax) and A_s(eq) reflect the 3d(Fe)–2s(F) hybridization describing the two unpaired electrons lying in the $3z^2 - r^2$ and $x^2 - y^2$ levels. Due to the C_{4v} symmetry of the centre, there is also a zero-field splitting term (equation (7)) in the spin Hamiltonian. Efforts have been made to obtain information on the local structure from the D parameter in equation (7) through the superposition model [71–73].

In table 4 are collected the values of A_s(ax) and A_s(eq) in the $KMgF_3$ [68] lattice together with the A_s value for the FeF_6^{3-} complex in the *same* lattice [218]. As A_s(eq) = 72.3 MHz while A_s = 71.2 MHz for $KMgF_3$:Fe^{3+}, these results would support a slight contraction of the equatorial distance on passing from FeF_6^{3-} to $FeOF_5^{4-}$ in $KMgF_3$ *provided* the law embodied in equation (10) is true in C_{4v}. In particular, assuming equation (10) and taking R = 1.93 Å for the cubic centre in $KMgF_3$: Fe^{3+} [30] there is obtained R_{eq} = 1.92 Å and R_{ax} = 2.20 Å (table 5). This conclusion, similar to that obtained by Siegel and Muller [71], is hard to accept because

Table 5. Values (in Å) of the three metal–ligand distances of $FeOF_5^{4-}$ in $KMgF_3$ obtained through different procedures.

Method	R_{eq}	R_{ax}	R_0	References
Analysis of D through superposition model	1.88	2.01	1.95	[72]
	1.94	2.02	1.80	[73]
Analysis of $A_s(ax)$ and $A_s(eq)$ using equation (10)	1.92	2.20	—	[76]
DFT calculation on a 21 atom cluster	2.03	2.09	1.83	[76, 74]
DFT calculation on a 57 atom cluster	2.02	2.05	1.81	[76, 74]

the formation of a Fe^{3+}–O^{2-} *pair* would favour an increase of both R_{eq} and R_{ax} distances with respect to $R = 1.93$ Å for FeF_6^{3-} in $KMgF_3$. DFT calculations [74, 76] have shed some light on this puzzling problem, giving $R_{eq} = 2.02$ Å and $R_{ax} = 2.05$ Å in the biggest employed cluster (table 5). These values are consistent with an outwards relaxation of *both* equatorial and axial ligands and a difference between R_{eq} and R_{ax} much smaller than that derived through equation (10). The failure of equation (10) to provide reasonable values of R_{eq} and R_{ax} lies again in the different nature of the $\sim 3z^2 - r^2$ orbital on passing from O_h to C_{4v} symmetry. As shown in equation (23), the 3d–4s hybridization is allowed under an $F^- \rightarrow O^{2-}$ substitution. This process produces an extra *negative* charge on an axial ligand. Therefore, the energy of a $\sim 3z^2 - r^2$ electron is decreased by enhancing its probability of being in the perpendicular xy plane rather than along the z axis. In the present case, this means that the admixture factor ε in equation (23) is negative and thus favours that $A_s(eq) > A_s(ax)$ *even* if $R_{eq} = R_{ax}$ [74, 76]. Calculated values of the ratio $A_s(eq)/A_s(ax)$ are reasonably close to the experimental figure $A_s(eq)/A_s(ax) = 2.3$ for $FeOF_5^{4-}$ in $KMgF_3$ [68, 76]. On the other hand, if O^{2-} is replaced by an F^- vacancy it is found that $A_s(eq)/A_s(ax) = 0.86$ [76]. This is quite reasonable since the replacement of F^- by a vacancy favours that $\varepsilon > 0$ and thus $A_s(eq) < A_s(ax)$.

Results gathered in table 5 cast serious doubts about the reliability of the superposition model [220] widely used for deriving information on the local structure from the zero-field splitting parameter, D. It is worth noting that this model is based on two hard assumptions [162]: (i) the six bonds involved in a complex like $FeOF_5^{4-}$ can be treated *independently*, the value of D being the sum of quantities associated with all bonds; (ii) the properties of a single bond are the same independently of the symmetry of the complex as a whole. The first assumption is wrong when there is chemical bonding between the impurity and ligands. Nevertheless, it can be more reasonable in cases when ligands can be well approximated by point charges and thus the CF theory is not a bad description. Thus, this situation can hardly be true in the realm of 3d impurities but might happen for trivalent rare earth impurities.

4.2. Modifications due to electric fields from the rest of the lattice ions

4.2.1. Comparison between K_2NaCrF_6 and CrF_3: does $10Dq$ follow R? Optical experiments on K_2NaCrF_6 and CrF_3 compounds gave some surprising results [221, 222]. Such compounds involve CrF_6^{3-} units whose R values are well known through standard x-ray diffraction methods: $R = 1.93$ Å for K_2NaCrF_6, while the figure for CrF_3 ($R = 1.90$ Å) is slightly smaller. The optical absorption in the visible region is governed by the absorption of CrF_6^{3-} complexes and from the first spin allowed $^4A_{2g} \rightarrow {}^4T_{2g}$ transition the following $10Dq$ values are derived: 16 100 cm^{-1} for K_2NaCrF_6, while it is *only* 14 650 cm^{-1} for CrF_3. These results can hardly be understood through equation (9) with a positive value of the exponent n. Calculations carried out by Pierlot *et al* [222] demonstrated that this amazing result can be well explained

once the effects on the CrF_6^{3-} complex of the *different* V_R potential in the two lattices are taken into account. In essence, while V_R is found to be almost flat for K_2NaCrF_6, $(-e)V_R$ in CrF_3 decreases the energy of electrons lying on ligands. As this effect is thus bigger for e_g electrons with σ character than for t_{2g} this leads to a reduction of $10Dq$. If this explanation is right for a compound like CrF_3 where a ligand is *shared* by adjacent complexes it should be more valid when truly isolated impurities are involved. Along this line in the CT spectrum of $CuBr_4(NH_3)_2^{2-}$ inserted in NH_4Br the energy of the first $Br^- \rightarrow Cu^{2+}$ transition is measured to be only 6000 cm^{-1} higher than the corresponding to the NH_3 ligand [223]. This difference (certainly smaller than ∼15 000 cm^{-1} estimated from the optical electronegativity scale [131]) can however be explained by considering the effects of V_R upon the complex [47]. As shown in figure 3, V_R reduces the separation between 2p levels of nitrogen and 3p levels of bromine ligands.

4.2.2. Colour in gemstones: the puzzle of ruby and emerald. The ideas developed in sections 2.3 and 4.2.1 can be of help for explaining the colour of gemstones where the impurity is located in low-symmetry places. In this domain recent progress [227] has been made for solving the puzzling problem of the difference in colour between ruby (Al_2O_3:Cr^{3+}) and emerald ($Be_3Si_6Al_2O_{18}$:Cr^{3+}) [2, 9–11]. In both gemstones the colour is due to CrO_6^{9-} units formed under the $Al^{3+} \rightarrow Cr^{3+}$ substitution. The local symmetry is D_3 in emerald but only C_3 in ruby [10, 224]. In an approximate O_h description, the first excited state (from which emission originates) is $^2E_g(t_{2g}^3)$ while the absorption in the visible comes from the spin allowed $^4A_{2g}(t_{2g}^3) \rightarrow {}^4T_{2g}(t_{2g}^2e_g)$ and $^4A_{2g} \rightarrow {}^4T_{2g}(t_{2g}^2e_g)$ transitions. The sharp $^2E_g(t_{2g}^3) \rightarrow {}^4A_{2g}(t_{2g}^3)$ emission appears at 14 690 cm^{-1} for emerald while for ruby the corresponding energy is *only* 1.8% *smaller* [182, 225]. However, much bigger differences are observed in the absorption spectrum. In fact, the $^4A_{2g}(t_{2g}^3) \rightarrow {}^4T_{2g}(t_{2g}^2e_g)$ transition is measured at 16 130 cm^{-1} for emerald and at 18 070 cm^{-1} for ruby, leading to their characteristic green and red colours, respectively [9–11]. Attempts have been made to explain this remarkable difference through the ligand field theory assuming that [226, 2, 9–11]: (i) the *average* Cr^{3+}–O^{2-} distance, R, is different in both gemstones; (ii) the energy of the $^4A_{2g}(t_{2g}^3) \rightarrow {}^4T_{2g}(t_{2g}^2e_g)$ transition, equal to $10Dq$, follows the R dependence of equation (9).

Under these assumption the average Cr^{3+}–O^{2-} distance for ruby should then be ∼5 pm smaller than for emerald. However, this conclusion is not easy to accept because the Al^{3+}–O^{2-} distance in $Be_3Si_6Al_2O_{18}$ is 1.903 Å, and is thus a little smaller than the corresponding *average* distance in Al_2O_3 ($R = 1.915$ Å) [224]. Thus, according to results on impurities in insulating lattices (sections 2.4, 3.1.1 and 3.1.2) one would expect that the average Cr^{3+}–O^{2-} distance in both gemstones is practically the same. This statement has recently been verified by EXAFS measurements on both gemstones, leading to $R = 1.97$ Å [92, 224].

In another interpretation based on the CF approximation, however, a higher ionicity is assumed for the Cr^{3+}–O^{2-} bond in Al_2O_3 than in $Be_3Si_6Al_2O_{18}$ [9, 224]. This would imply a higher $|z_L|$ value in (18) for ruby than for emerald, thus explaining, albeit qualitatively, the bigger $10Dq$ value of ruby. Nevertheless, a higher covalence in emerald than in ruby would also imply that the energy of the $^2E_g(t_{2g}^3) \rightarrow {}^4A_{2g}(t_{2g}^3)$ transition is higher for the former than for the latter, a conclusion which is against experimental evidence.

The difference in colour between ruby and emerald can be reasonably accounted for once the influence of the V_R potential on the CrO_6^{9-} complex is considered [227]. From the discussion in sections 2.3 and 4.2.1, the parameter $10Dq$ can be written as

$$10Dq = [10Dq(R)]_v + \Delta_R. \tag{25}$$

Here $[10Dq(R)]_v$ just means the $10Dq$ value corresponding to a complex *in vacuo* but at the

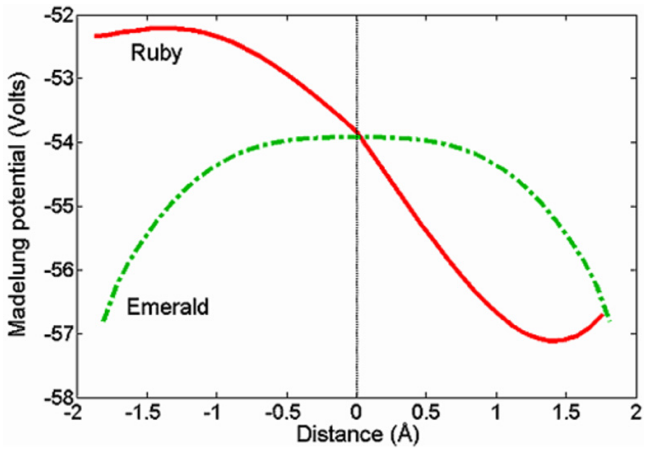

Figure 9. Madelung potential, $V_R(x)$, on CrO_6^{9-} along metal–ligand directions for ruby and emerald host lattices. Data are taken from [227].

Table 6. Calculated values of $10Dq$, $[10Dq]_v$ and Δ_R (defined in equation (25)) at the equilibrium geometry of the CrO_6^{9-} unit for ruby and emerald. Data are taken from [227]. The experimental $10Dq$ value [9, 10, 224] is given for comparison. All values are in cm^{-1}.

	$[10Dq]_v$	Δ_R	$10Dq$	$10Dq$ (exp.)
Emerald	16 188	−449	15 739	16 130
Ruby	16 043	2136	18 179	18 070

right experimental distance. The quantity Δ_R depicts the correction due to V_R which in turn reflects the different effect of such a potential upon e_g and t_{2g} orbitals. Calculated $[10Dq(R)]_v$ and Δ_R values using the experimental Cr^{3+}–O^{2-} distances (table 6) demonstrate that Δ_R is the main factor responsible for the different colour of both gemstones [227]. The main effect of V_R appears in ruby and it can be rationalized by looking at the picture of such a potential given in figure 9. According to the low C_3 symmetry, there is an electric field around Cr^{3+} (along the metal–ligand directions) which is however absent in emerald, consistently with its D_3 local symmetry.

It is worth noting that V_R has much less importance as far as the $^2E_g(t_{2g}^3) \rightarrow {}^4A_{2g}(t_{2g}^3)$ emission in such gemstones is concerned since the involved states both arise from the *same* configuration [227]. This simple reasoning is consistent with the fact that the energy of the emission lines in ruby and emerald only differ by 1.8% [225]. It should be noticed that V_R can also modify (but only slightly) the covalence in the t_{2g} orbital, thus leading to changes of Racah parameters and emission energy. A deviation of 3.5% with respect to the emission energy in ruby has been reported for $LiSc(WO_4)_2$:Cr^{3+} [228].

5. Jahn–Teller instabilities in the ground state of impurities

5.1. Jahn–Teller effect in cubic crystals: the $E \otimes e$ problem

Strictly speaking, the JT instability appears when the ground state of a substitutional impurity is orbitally degenerate in the local symmetry of the host lattice [113, 229]. For octahedral symmetry this happens for d^9 ions, d^7 ions in the low-spin configuration, and d^4 ions in the

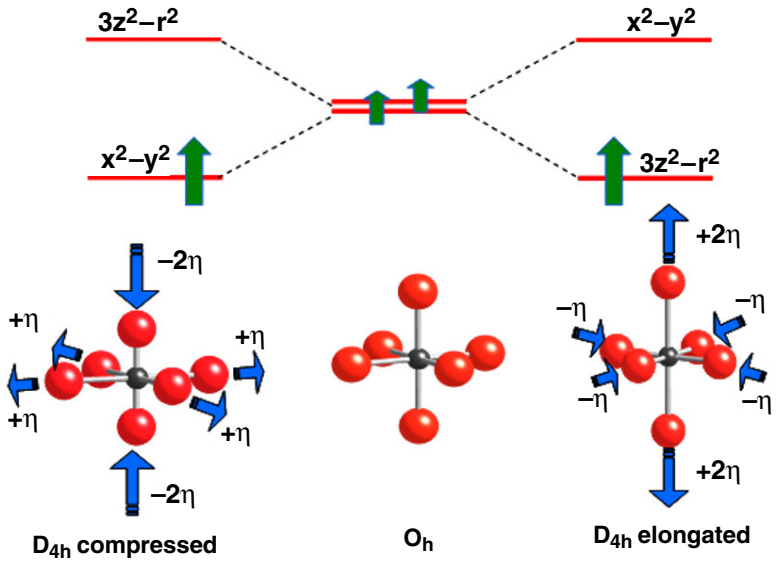

Figure 10. Level scheme for the octahedral reference configuration (centre), tetragonal elongated (right) and compressed (left) geometries corresponding to a d^7 impurity in strong field situation. The value of Q_θ for an elongated situation is equal to $\sqrt{12}\eta$.

high-spin one. In all cases the E_g ground state has an unpaired electron with σ character. This state can be coupled to the *stretching* e_g mode of the MX_6 complex (figure 10) described by the normal coordinates $Q_\theta \sim 3z^2 - r^2$ and $Q_\varepsilon \sim x^2 - y^2$, or equivalently by the polar coordinates ρ and φ defined through

$$Q_\theta = \rho \cos\varphi; \qquad Q_\varepsilon = \rho \sin\varphi. \tag{26}$$

The present section will only be focused on the so-called $E \otimes e$ problem. It is worthwhile noting that $3d^6$ and $3d^7$ impurities in octahedral symmetry and high-spin configuration have an orbital triplet ground state [83]. This situation is often found in *excited* states of O_h complexes involving d^3, d^5 or d^8 ions and is discussed on section 7.

5.1.1. Description through a model Hamiltonian. Let us designate by R_{OC} the equilibrium distance of an MX_6 complex when the octahedral symmetry *is* kept, and by H_0 the corresponding static Hamiltonian. The existence of adiabatic minima involving a small e_g distortion requires us first to explore [113, 229]

$$H = H_0 + H_{LV}; \qquad H_{LV} = V_\theta(\mathbf{r})Q_\theta + V_\varepsilon(\mathbf{r})Q_\varepsilon \tag{27}$$

where H_{LV} depicts the linear $E \otimes e$ vibronic interaction. This term *keeps the cubic* symmetry provided symmetry operations are performed on *both* the electronic, $\mathbf{r}$, and vibrational, Q_θ and Q_ε, coordinates.

A central concept in the JT effect is the *reference state* [33, 94]. For the sake of clarity let us consider a d^7 ion in octahedral symmetry and $S = 1/2$. Although the actual ground state is orbitally degenerate, there can be imagined as a first step an electronic configuration which is orbitally a singlet. This artificial configuration can easily be built in the domain of DFT by placing half an electron in both the $x^2 - y^2$ and $3z^2 - r^2$ orbitals with parallel spins. Thus the $(3z^2 - r^2)^{0.5}\ (x^2 - y^2)^{0.5}$ configuration with fractional occupation is similar to the A_{2g} ground state of a d^8 impurity in octahedral symmetry [83]. As is shown in figure 10, an

elongation of the octahedron along the OZ axis would produce an increase (decrease) of the energy of the x^2-y^2 ($3z^2-r^2$) level and thus no variation of the total energy for this $(3z^2–r^2)^{0.5}$ $(x^2-y^2)^{0.5}$ configuration. This fact simply reflects that $E_g \not\subset A_{2g} \otimes A_{2g}$ and thus the ground state energy around $Q_\theta = Q_\varepsilon = 0$ can simply be written as

$$E = E_{OC} + \tfrac{1}{2}M_L\omega_e^2(Q_\theta^2 + Q_\varepsilon^2) + \cdots \tag{28}$$

where M_L is the ligand mass. Nevertheless, when the whole electron is placed in the $3z^2-r^2$ orbital the ground state electronic energy can be lessened through a Q_θ type distortion (figure 10) described by equation (22). The non-symmetric distortion which appears on passing from the reference state to the $(3z^2-r^2)^1$ configuration can easily be understood by looking at forces on ligands induced by *changes* of electronic density [230]. Let us call n_{JT} the *variation* of the electronic density on going from $(3z^2-r^2)^{0.5}$ $(x^2-y^2)^{0.5}$ to $(3z^2-r^2)^1$. It is equal to

$$n_{JT} = \tfrac{1}{2}[n_{3z^2-r^2} - n_{x^2-y^2}]; \qquad n_{3z^2-r^2} \sim (3z^2-r^2)^2; \qquad n_{x^2-y^2} \sim \left[\sqrt{3}(x^2-y^2)\right]^2. \tag{29}$$

Here $n_{3z^2-r^2}$ means the electronic density corresponding to a $\sim 3z^2 - r^2$ wavefunction. Therefore, the differential density

$$n_{JT} \sim 2z^4 - (x^4+y^4) + 4x^2y^2 - 2z^2(x^2+y^2) \tag{30}$$

at $(0, 0, u)$ is just *twice* that at $(u, 0, 0)$ or $(0, u, 0)$ and of *different* sign [230]. This implies that the electrostatic force associated with n_{JT} is pulling inwards the equatorial ligands while pushing outwards the axial ones, thus generating the Q_θ distortion of figure 10.

Let us now consider the effects of H_{LV} in equation (27), but only within *the frozen* $\{3z^2-r^2, x^2-y^2\}$ basis corresponding to H_0. This gives rise to the following effective Hamiltonian, H_{eff} [113, 229]:

$$\begin{aligned} &H_{eff} = E_{OC} + V_{1e}(\mathbf{U}_\theta Q_\theta + \mathbf{U}_\varepsilon Q_\varepsilon) + V_{2a}(Q_\theta^2 + Q_\varepsilon^2)\mathbf{I} \\ &2V_{2a} \equiv M_L\omega_e^2; \qquad \mathbf{U}_\theta = \begin{pmatrix} -1 & 0 \\ 0 & 1 \end{pmatrix}; \qquad \mathbf{U}_\varepsilon = \begin{pmatrix} 0 & 1 \\ 1 & 0 \end{pmatrix}. \end{aligned} \tag{31}$$

Here, V_{1e} reflects the decrease of electronic energy by elongating the octahedron and placing the electron in $3z^2-r^2$. However, it should be remarked that the *same* energy gain can be obtained by placing the electron in x^2-y^2 and compressing the octahedron (figure 10). Furthermore, the adiabatic solutions of the two states described by (31) are [113, 229]

$$\begin{aligned} &E_\pm(\rho;\varphi) = E_{OC} \pm V_{1e}\rho + V_{2a}\rho^2 \\ &\Psi_-(\rho;\varphi) = \cos\frac{\varphi}{2}|3z^2-r^2\rangle - \sin\frac{\varphi}{2}|x^2-y^2\rangle \\ &\Psi_+(\rho;\varphi) = \sin\frac{\varphi}{2}|3z^2-r^2\rangle + \cos\frac{\varphi}{2}|x^2-y^2\rangle. \end{aligned} \tag{32}$$

Thus, the equilibrium situations found for the lower branch are

$$\rho_0 = \frac{V_{1e}}{M_L\omega_e^2}; \qquad E_{JT} = -\frac{1}{2}V_{1e}\rho_0. \tag{33}$$

Equation (33) just means that distortions described by the circle $\rho = \rho_0$ are all equivalent. This conclusion is a bit puzzling as it does not reflect the actual cubic symmetry of the problem shown by equation (31). However, strict cubic symmetry is recovered once the anharmonicity in the e_g mode (inevitably present, as for any molecular vibration) is considered [231, 232, 94], by adding a new H_{anh} term to the effective Hamiltonian (31)

$$H_{anh} = V_{3a}(Q_\theta^3 - 3Q_\theta Q_\varepsilon^2). \tag{34}$$

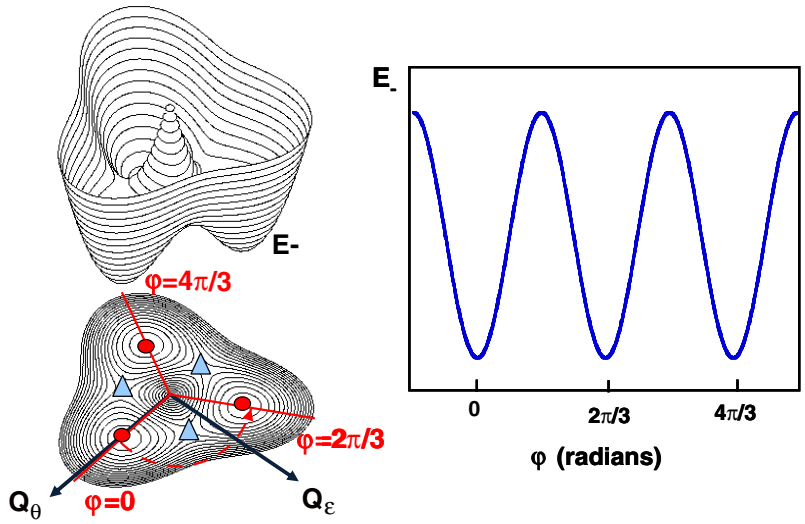

Figure 11. Left: adiabatic potential energy surface shape for the JT effect, called the 'Tricorn' or warped 'Mexican hat', showing the positions of three minima (circles) and saddle points (triangles) Right: variation of the ground state energy, E_-, with the φ angle, alternating minima and saddle points.

For an *isolated* MX_6 complex one would expect $V_{3a} < 0$, because it is easier to elongate rather than to compress the axial bonds in a $Q_\varepsilon = 0$ and $Q_\theta \neq 0$ distortion (figure 10). Once the H_{anh} term is included in equation (32), the adiabatic energy for the lowest branch becomes

$$E_- = E_{OC} - V_{1e}\rho + V_{2a}\rho^2 + V_{3a}\rho^3 \cos 3\varphi. \tag{35}$$

If $V_{3a} > 0$, at equilibrium there are three D_{4h} distortions (characterized by $\rho \approx \rho_0$ and $\varphi = 0, \pm 2\pi/3$) which are fully equivalent, consistently with the cubic symmetry of (31) and (35). The C_4 axis of the three distortions (called OZ') is thus parallel to one of the crystal cubic axes $\{OX, OY, OZ\}$. For passing from $\varphi = 0$ to $\varphi = \pm 2\pi/3$ there is now an energy barrier B [232]

$$B \approx 2\rho_0^3 V_{3a}. \tag{36}$$

If $V_{3a} > 0$, the maximum of the barrier corresponds to $\varphi = \pi, \pm\pi/3$, where $\varphi = \pi$ depicts a compressed octahedron with an $x^2 - y^2$ unpaired electron (figure 11). For a D_{4h} distortion ($Q_\varepsilon = 0$, $Q_\theta = \rho_0$) described by (22), the relation between ρ_0 and η is given by

$$\rho_0 = \sqrt{12}\eta. \tag{37}$$

As η typically lies in the 0.05–0.2 Å range and $V_{3a} \sim 1$ eV Å^{-3} [231, 94], it turns out that the barrier B is expected to lie in the 10–1000 cm^{-1} range. A recent study on several $E \otimes e$ systems has shown that usually H_{anh} is the main factor responsible for the warping of the $E(\rho, \varphi)$ surface at least working at zero pressure [94].

Let us now consider the three wavefunctions, $\{\Phi_X, \Phi_Y, \Phi_Z\}$ associated with the equivalent minima in figure 11:

$$\Phi_X = |3x^2 - r^2\rangle|\chi(2\pi/3)\rangle; \qquad \Phi_Y = |3y^2 - r^2\rangle|\chi(4\pi/3)\rangle;$$
$$\Phi_Z = |3z^2 - r^2\rangle|\chi(0)\rangle. \tag{38}$$

Here, $\chi(\varphi)$ depicts the lowest vibrational state corresponding to the three minima at $\varphi = 0, \pm 2\pi/3$. Going beyond the adiabatic approximation, the right wavefunction should actually

be a linear combination of three, Φ_X, Φ_Y and Φ_Z, thus implying the existence of *coherent tunnelling*. This phenomenon, first predicted by Bersuker [113], is of current interest for quantum information processing [233]. In this situation the ground state is a *vibronic* E_g doublet while the first excited state is a singlet A_{1g} state. Such states are depicted by

$$|\theta\rangle = \frac{1}{\sqrt{6}}\{2\Phi_Z - \Phi_X - \Phi_Y\}; \qquad |\varepsilon\rangle = \frac{1}{\sqrt{2}}\{\Phi_X - \Phi_Y\};$$
$$|A_{1g}\rangle = \frac{1}{\sqrt{3}}\{\Phi_Z + \Phi_X + \Phi_Y\}. \tag{39}$$

The separation between both states, called 3Γ, reflects the tunnelling splitting which increases when the energy barrier B does. Typically, 3Γ is estimated to be $\sim$1 cm^{-1} [113, 229]. The interaction of this vibronic E_g doublet with an external magnetic field, **H**, is similar to that of a purely electronic doublet described through $\{x^2 - y^2, 3z^2 - r^2\}$ wavefunctions [139]. The angular dependence of g factors related to the two Kramers doublets is [113, 229]

$$g_\pm = g_1 \pm g_2[1 - 3(n_x^2 n_y^2 + n_x^2 n_z^2 + n_y^2 n_z^2)]^{1/2}; \qquad g_1 = g_0 + \frac{4\xi}{(10Dq)}; \qquad g_2 = q\frac{4\xi}{(10Dq)}. \tag{40}$$

Here $n = \mathbf{H}/|\mathbf{H}|$ and $q = 1$ for the electronic $\{x^2 - y^2, 3z^2 - r^2\}$ doublet while $q = 1/2$ for the vibronic one when overlap integrals like $\langle\chi(2\pi/3)|\chi(0)\rangle$ are neglected. For this situation the *reduction* factor $q = 1/2$ can easily be obtained by computing

$$q = \frac{\langle\theta|L_z^2 - L^2/3|\theta\rangle}{\langle 3z^2 - r^2|L_z^2 - L^2/3|3z^2 - r^2\rangle}, \tag{41}$$

where $|\theta\rangle$ is defined in (39).

Similarly to equation (5), the expressions of g_1 and g_2 in (40) are valid for an ionic complex. The angular pattern of equation (40) is consistent with the cubic symmetry of the model Hamiltonian described by equations (31), (34) and (35).

As was first pointed out by Ham [229], EPR spectra of JT impurities showing a tetragonal rather that a cubic angular pattern come from random strains which are *unavoidable* in any *real* crystal. In fact, linear and point defects are necessary for growing a crystal [234, 14]. Let us now consider the $e_{\theta\theta} \sim 3z^2 - r^2$ and $e_{\varepsilon\varepsilon} \sim x^2 - y^2$ strains defined in the local $\{X', Y', Z'\}$ coordinate system as

$$e_{\theta\theta} = 2e_{Z'Z'} - (e_{X'X'} + e_{Y'Y'}); \qquad e_{\varepsilon\varepsilon} = \frac{\sqrt{3}}{2}(e_{X'X'} - e_{Y'Y'}). \tag{42}$$

In accordance with (31), an $e_{\theta\theta}$ strain (behaving like $-Q_\theta$) produces, in first order, a shift of the ground state equal to $(2/\sqrt{3})R_{OC}e_{\theta\theta}V_{1e}$. By contrast, no first-order effect comes from the $e_{\varepsilon\varepsilon}$ strain [229]. As typical random strains are $\sim 10^{-4}$, the energy shift of the ground state can be comparable to or higher than 3Γ and then the coherence among Φ_X, Φ_Y and Φ_Z in equation (39) is destroyed [229]. In this case, the non-equivalence of the three minima in figure 11 caused by random strains can lock the system in one of the three wells.

Just around the minima of these wells (described by equation (35)) the adiabatic energy $E(\rho_0, \varphi)$ can be approximated by [232]

$$E \simeq E(\rho_0, \varphi_0) + \tfrac{1}{2}M_L\omega_\varphi^2(\varphi - \varphi_0)^2; \qquad \omega_\varphi^2 = 9V_{3a}\rho_0^3 \tag{43}$$

where $\varphi_0 = 0, \pm 2\pi/3$. Obviously, coherent tunnelling is favoured by a decrease of the F parameter defined by [94]

$$F = B/(\hbar\omega_\varphi/2). \tag{44}$$

It is worth noting here that random strains are also responsible for the inhomogeneous broadening of zero-phonon lines [59].

5.1.2. Phenomena related to the Jahn–Teller effect: experimental information. Low-temperature EPR spectra provide us with relevant experimental information on the ground state of E ⊗ e JT impurities in cubic insulators [31]. In the analysis of EPR data it is necessary to clarify two crucial questions. (i) The nature of adiabatic minima. In the case of octahedral coordination this means knowing what conformation (elongated or compressed) is the stable one. (ii) The angular pattern displayed by EPR spectra. An angular pattern following equation (40) supports the existence of coherent tunnelling, while if [**g**] and hyperfine tensors exhibit a tetragonal pattern it means that random strains are able to lock the system in one of the three wells which are no longer equivalent. This situation is briefly called a *static* JT effect [113].

In the realm of the E⊗e JT coupling, d^9 impurities have been explored in cubic lattices like alkali and silver halides, fluoroperovskites, and oxides like MgO or SrO [31, 34, 35, 235–239]. Also some attention has been addressed to d^7 ions in low-spin configuration in alkali and silver halides [31, 32, 213]. Apart from these cases involving an octahedral coordination, other interesting E ⊗ e systems concern d^1 ions (like Sc^{2+} or La^{2+}) in cubic coordination [239].

Low-temperature EPR spectra of Cu^{2+}, Ag^{2+} and Rh^{2+} in alkali and silver halides with *remote* charge compensation show a tetragonal angular pattern typical of a static JT effect, the C_4 axis being one of the three principal cubic axes [31, 32, 34, 238]. Therefore for a general orientation of the magnetic field, **H**, the EPR spectrum is a superposition of three different spectra reflecting the angle between **H** and the three OX, OY and OZ axes. As strains are randomly distributed inside the crystal the concentration of these *three centres* is the same. For Cu^{2+}- and Ag^{2+}-doped alkali and silver halides and fluoroperovskites it is usually found that $g_\parallel - g_0 > g_\perp - g_0$, implying that the unpaired electron lies in the $x^2 - y^2$ orbital and thus the ligand octahedron is elongated. In the case of d^7 ions (as Rh^{2+}, Ir^{2+} or Pd^{3+}) EPR results give $g_\parallel - g_0 < g_\perp - g_0$, consistent with a location of the unpaired electron in the $3z^2 - r^2$ orbital but again an elongated equilibrium geometry [31, 32, 213].

EPR spectra with $g_\parallel = 2.06$ and $g_\perp = 2.4$ observed for x-irradiated samples of LiF and NaF doped with Ni^{2+} were attributed to the formation of *compressed* NiF_6^{5-} complexes [240]. However, subsequent theoretical [241] and experimental [242] work showed that such spectra can hardly be assigned to NiF_6^{5-} complexes. JT NiF_6^{5-} species have been formed in several cubic fluoroperovskites and in all cases it is found that $g_\parallel - g_0 > g_\perp - g_0$, thus implying an elongated geometry [165, 243].

Relevant systems for establishing present ideas on the JT effect were obtained in the study of Cu^{2+}-doped cubic oxides. Coffman's results on MgO:Cu^{2+} and CaO:Cu^{2+} [235, 236] showed for the first time that EPR spectra of a E ⊗ e system do not *necessarily* display a tetragonal symmetry but can follow the cubic pattern of equation (40). For MgO:Cu^{2+} the experimental $g_1 = 2.195$ and $g_2 = 0.108$ values [235] are consistent with a reduction factor $q \approx 0.5$. The cubic pattern depicted by equation (40) was also encountered for d^1 ions in fluorite type lattices [239, 229].

As regards d^9 ions in cubic oxides, the cubic pattern of equation (40) is also observed for MgO:Ag^{2+} but not for Cu^{2+}- and Ag^{2+}-doped SrO and CaO:Ag^{2+} where the pattern is tetragonal [35]. Furthermore, the experimental [**g**] tensor shows that the equilibrium geometry is elongated for SrO:Ag^{2+} [35] but compressed for SrO:Cu^{2+} [237]. A compressed geometry has also been inferred for CaO:Cu^{2+} from Raman spectra corresponding to vibronic levels [244].

In accord with the analysis of section 5.1.1, the nature of the observed effect depends on random strains and thus can be sensitive to crystal growth. Some influence of crystal growth on EPR spectra has been found by Schoenberg *et al* [245].

Although in a *static* JT effect random strains destroy the coherence involved in equation (39), low barriers among the three wells of figure 11 make possible the existence

of *incoherent hopping* [31, 113, 229]. Two main facts related to this phenomenon are: (i) the change of relative intensity of EPR lines due to an applied uniaxial stress; (ii) the transition from a static spectrum to an averaged one when the temperature increases.

Let us now consider as a guide an $e_{ZZ} = \zeta > 0$ *external* strain on a cubic crystal containing a d^7 impurity in a static situation. For centres having $OZ' = OZ$ this means $e_{\theta\theta} = \zeta$, and according to (31) an increase of the energy of the $3z^2 - r^2$ orbital. By contrast, for centres with $OZ' = OX$ or OY a value $e_{\theta\theta} = -\zeta/2$ is obtained from equation (42). This just means that the difference of the ground state energy among $OZ' = OZ$ and $OZ' = OX$ or OY centres is proportional to $3\zeta/2$ and thus at thermodynamic equilibrium the population of the former centres should decrease. However, for achieving thermodynamic equilibrium it is necessary that the system can jump from one well of figure 11 to another one in order to reorient the principal C_4 axis. EPR experiments on NaF:Ag^{2+} under an external e_{ZZ} strain and **H** parallel to $\langle 100 \rangle$ directions reveal [238] that the increase of the $g_\parallel$ signal at $T = 4.2$ K is 'instantaneous'.

The incoherent jump among the three wells of figure 11 can also lead to an average EPR spectrum when the temperature is raised [31, 113, 229]. If the jump frequency, ν_J, follows an Arrhenius law

$$\nu_J = \nu_o e^{-B/k_B T} \tag{45}$$

the averaging of parallel and perpendicular signals requires

$$(g_\parallel - g_\perp)\beta H \ll h\nu_J. \tag{46}$$

Even when (46) is not fulfilled, $h\nu_J$ can however be higher than the separation between two close superhyperfine lines and then an averaging can still be observed [165].

It is worth noting that when the temperature, T, increases but (46) is not yet fulfilled the observed $g_\parallel$ and $g_\perp$ signals can depend on T [232, 246, 247]. Looking at figure 11, a temperature increase means bigger departures from minima at $\varphi = 0$ and $\pm 2\pi/3$. But according to equation (32) this departure implies a vibronic admixture of $3z^2 - r^2$ and $x^2 - y^2$ orbitals.

5.1.3. Microscopic origin of the energy barrier. The advent of reliable calculations has shed light on the different phenomena related to the JT effect as well as on the actual values of parameters described in section 5.1.1. It is worth noting that, for a well studied system like CaO:Cu^{2+}, values of the JT energy, E_{JT}, inferred from the analysis of experimental results go from 300 cm^{-1} to about 8000 cm^{-1} [244, 248–251].

Information on d^9 ions (like Cu^{2+} or Ag^{2+}) in cubic oxides and NaCl:Rh^{2+} derived from *ab initio* calculations [171, 94] is collected in table 7. One can first notice the huge differences between the absolute values of the barrier energies, $|B|$, obtained for NaCl:Rh^{2+} ($|B| = 511$ cm^{-1}) and that for MgO:Cu^{2+}($|B| = 4$ cm^{-1}) or CaO:Cu^{2+} ($|B| = 20$ cm^{-1}). This result, together with the computed values of the F factor (defined in (44)) for NaCl:Rh^{2+} ($F = 6.4$), MgO:Cu^{2+} ($F = 0.11$) and CaO:Cu^{2+} ($F = 0.40$), favours the observation of a static JT effect in the first case and a coherent tunnelling for Cu^{2+}-doped MgO and CaO. Furthermore, the F factor for SrO:Cu^{2+} is found to be ~20 times bigger than that for MgO:Cu^{2+}. Along this line the $F = 2.3$ value obtained for SrO:Ag^{2+} is again much higher than $F = 0.32$ computed for MgO:Ag^{2+}. These results thus favour a transition to a static JT when MgO is replaced by SrO for both Cu^{2+} and Ag^{2+} impurities. This transition can partially be related to the big decrement experienced by the V_{2a} constant on passing from MgO:Cu^{2+} to SrO:Cu^{2+} which is not balanced by the decrease of the linear coupling constant, V_{1e}. Although the big difference between $V_{2a} = 7$ eV $Å^{-2}$ for MgO:Cu^{2+} and $V_{2a} = 1.1$ eV $Å^{-2}$ for SrO:Cu^{2+} is partially influenced by the quite different R_{OC} values in both systems (table 7),

Table 7. Values of different parameters for representative Jahn–Teller systems obtained through *ab initio* calculations. R_{OC} and ρ_0 are given in Å, E_{JT} and B in cm^{-1} while V_{ie} and V_{ia} constants ($i = 1, 2, 3$) are in $eV/Å^i$ units. The metal–ligand distance for the perfect host lattice, R_H, is also given for comparison. Results come from [171].

System	R_H	R_{OC}	ρ_0	E_{JT}	V_{1e}	V_{2a}	V_{3a}	B	F
NaCl:Rh^{2+}	2.82	2.53	0.276	1832	1.42	2.70	−1.25	−511	6.4
MgO:Cu^{2+}	2.107	2.15	0.087	494	1.08	6.97	0.65	4	0.11
CaO:Cu^{2+}	2.405	2.32	0.126	567	0.52	1.85	0.65	20	0.40
SrO:Cu^{2+}	2.584	2.46	0.19	914	0.51	1.12	0.93	98	2.4
MgO:Ag^{2+}	2.107	2.20	0.097	674	1.73	8.79	0.44	−18	0.32
SrO:Ag^{2+}	2.584	2.54	0.251	1100	0.97	1.91	0.29	71	2.13

it cannot however be explained by assuming that V_{2a} is proportional to R_{OC}^{-3}, as could be expected for an *isolated* ionic complex [14]. In the same vein, while V_{2a} for MgO:Cu^{2+} is about 3.5 times bigger than the value for NaCl:Rh^{2+} it is surprisingly found that $|V_{3a}|$ for the latter is about twice that for the former system. Moreover, V_{3a} is found to be negative for NaCl:Rh^{2+} while it is positive for Cu^{2+} in cubic oxides. This result [171, 252] concurs with the elongated equilibrium geometry reported for NaCl:Rh^{2+} [32] and the compressed one of SrO:Cu^{2+} [237] and CaO:Cu^{2+} [244]. All these relevant issues cannot however be understood by assuming that V_{2a} and V_{3a} *only* reflect the interaction of the impurity with ligands. Indeed they require considering the elastic coupling of the complex with close neighbours of the host lattice (section 2.4). In a ball-and-spring model (figure 5), the energy corresponding to M–X–A bonds can be written as [168, 171]

$$E = E_0 + (1/2)k(x_L - x_M - r_0)^2 + (1/2)k'(x_A - x_L - r_0')^2 + (1/6)g(x_L - x_M - r_0)^3 + (1/6)g'(x_A - x_L - r_0')^3. \quad (47)$$

Here x_M, x_L and x_A mean the position of the impurity, the ligand and the A ion lying in the same ⟨100⟩ direction, respectively, while r_0 and r_0' are parameters describing the two springs. If the impurity and the A ion are fixed, the energy changes induced by variations of the ligand around the equilibrium position, x_{L0}, can be approximately described by

$$E \approx E_0 + (1/2)(k + k')(x_L - x_{L0})^2 + (1/6)(g - g')(x_L - x_{L0})^3. \quad (48)$$

Therefore, comparing (31) and (34) with (47) one can approximate

$$2V_{2a} = k + k'; \qquad 12\sqrt{3}V_{3a} = g - g'. \quad (49)$$

Then, if the complex is elastically decoupled from the rest of the lattice ($k \gg k'$) it can be expected that $V_{3a} < 0$ because $g < 0$ for a normal bond. By contrast, as long as the relative importance of k' increases there is a *softening* of the anharmonicity constant, V_{3a}, which can become positive when $g' > g$ [171].

The calculated values of k and k' for NaCl:Rh^{2+} give $k'/k = 0.38$. This result points out that the $RhCl_6^{4-}$ complex is significantly decoupled from the rest of the lattice [94], a fact which is ultimately due to the substitution of the monovalent Na^+ ion by the divalent Rh^{2+}. This decoupling favours that $V_{3a} < 0$ and thus that there is an elongated geometry, in agreement with experiments [32]. However, a quite different situation is found for MgO:Cu^{2+} and SrO:Cu^{2+}, where the calculated k'/k ratio is equal to 3.3 and 2.2, respectively. In these cases where V_{2a} is dominated by k' it can also be expected that $V_{3a} > 0$ and thus that there is a compressed geometry. Systems involving Ag^{2+} ions appear to be in the border line. So, though $V_{3a} = 0.29$ eV $Å^{-3}$ found for SrO:Ag^{2+} is the lowest value of $|V_{3a}|$ in table 7, V_{3a} and

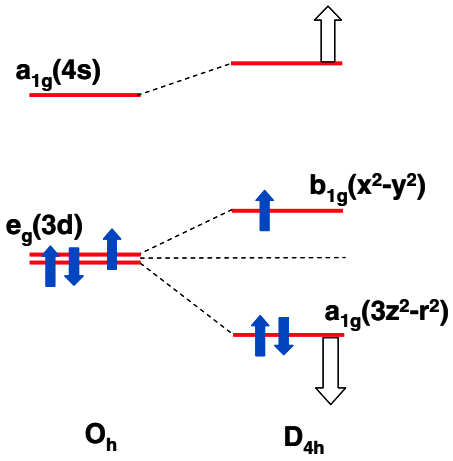

Figure 12. Splitting of the $e_g(3d)$ level under an $O_h \rightarrow D_{4h}$ distortion, and effect of the pseudo-JT interaction between a_{1g} $(3z^2 - r^2)$ and a_{1g} (4s) orbitals, depicted through white arrows.

B are, however, calculated to be positive. Nevertheless, experimental EPR data on this system indicate an elongated octahedral geometry [35].

It is worth noting now that there can be contributions to B that are different from the anharmonicity. In particular, excited states (not considered in section 5.1.1) can play a role in this issue [113, 94]. A mechanism involving an unoccupied $(n+1)$s level is depicted in figure 12 for an octahedral d^9 complex. In D_{4h} symmetry (but not in O_h) the $3z^2 - r^2$ orbital (but not $x^2 - y^2$) can be coupled to the $(n+1)$s level through the *linear* coupling operator V_θ (**r**) defined in (27). The repulsion between $3z^2 - r^2$ and the $(n+1)$s level induces a *supplementary* decrease of the energy of $3z^2 - r^2$, which is however proportional to Q_θ^2 [94]. The energy gain coming from this pseudo-JT mechanism is thus bigger if two electrons are located on this orbital rather than on $x^2 - y^2$, favouring again an elongated situation. Obviously, if the dominant interaction of $3z^2 - r^2$ through $V_\theta(\mathbf{r})$ is with an a_{1g} filled bonding orbital this mechanism alone would enhance a compressed geometry.

Although in the $E \otimes e$ JT systems discussed up to now the anharmonicity appears to be the main factor responsible for the barrier [171, 94], this is not necessarily true. In fact, the energy barrier is proportional only to Q_θ^2 for the pseudo-JT mechanism and thus this mechanism could dominate when the distortion becomes smaller due to an applied pressure.

5.2. Jahn–Teller effect in non-cubic crystals: the influence of V_R

The machinery of the $E \otimes e$ JT effect has also been employed in trying to rationalize the experimental results of d^9 impurities in lower symmetry lattices. So, for explaining the results on K_2ZnF_4:Cu^{2+} the formalism of section 5.1.1 has been used, though adding a phenomenological internal strain which destroys the equivalence of the three wells depicted in figure 11 [108, 246]. A similar scheme has been employed in connection with $CuCl_4(H_2O)_2^{2-}$ centres [108, 253]. However, in the tetragonal $CuCl_4X_2^{2-}$ (X: H_2O; NH_3) complexes with two different kinds of ligand it is hard to imagine an electronic ground state with orbital degeneracy as a starting point [47].

The comparison of EPR results derived for K_2ZnF_4:Cu^{2+} [108, 246] and K_2MgF_4:Ni^+ [254] is certainly puzzling and can hardly be ascribed to a different internal strain in both systems. Indeed, the two host lattices, K_2ZnF_4 and K_2MgF_4 (figure 13), are

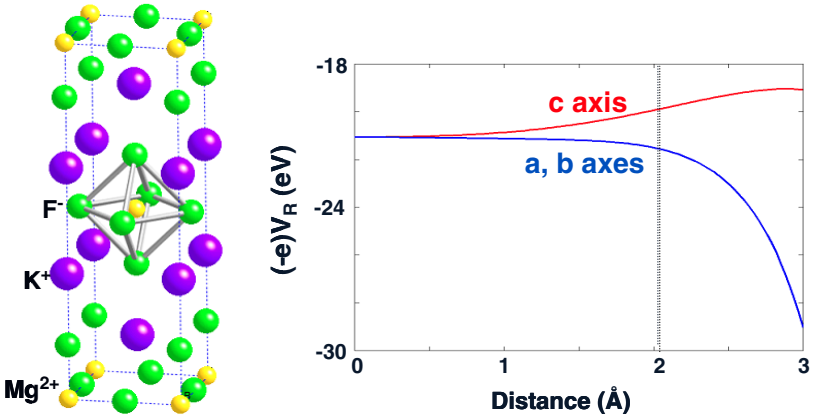

Figure 13. Left: unit cell of the K_2MgF_4 lattice and coordination polyhedron of Mg^{2+}. Right: electrostatic potential, V_R, of the rest of the lattice along [100] and [001] directions on a seven-atom cluster. The divalent cation is at the origin.

isomorphous while Cu^{2+} and Ni^{+} are isoelectronic. Furthermore, the six neighbour F^{-} ions of the divalent cation display a practically perfect octahedron for both K_2ZnF_4 and K_2MgF_4 lattices. In fact, calling R^{h}_{ax} and R^{h}_{eq} the axial and equatorial B^{2+}–F^{-} distances (B = Zn, Mg) for the host lattice, then $R^{h}_{ax} = 2.03$ Å and $R^{h}_{eq} = 2.02$ Å for K_2ZnF_4, while $R^{h}_{ax} = 2.00$ Å and $R^{h}_{eq} = 1.99$ Å for K_2MgF_4 [255, 127]. Despite all these similarities, EPR data prove that the unpaired electron is placed in the $3z^2 - r^2$ orbital (OZ being parallel to the crystalline C_4 axis) for K_2ZnF_4:Cu^{2+} [108, 246] while it is lying in the $x^2 - y^2$ orbital for K_2MgF_4:Ni^{+} [254].

A first key for understanding this puzzling situation is to consider the electronic structure of both impurities *imposing* octahedral geometry, that is making $R_{ax} = R_{eq}$. As a salient feature it is found that for K_2MgF_4:Cu^{2+} at $R_{ax} = R_{eq} = 2.02$ Å the two $3z^2 - r^2$ and $x^2 - y^2$ levels are *not degenerate* but $x^2 - y^2$ is the lowest and there is a separation, $\Delta_O = 0.39$ eV, between them [255]. Once again, this gap between A_{1g} and B_{1g} states comes from the action of the tetragonal field due to the rest of the lattice, V_R, on the CuF_6^{4-} complex. It is worth noting that $(-e)V_R$ is smaller when the electron lies in [100] or [010] directions than when it is located along the **c** crystal axis (figure 13). Therefore, V_R makes the energy of the $3z^2 - r^2$ orbital higher than that corresponding to the $x^2 - y^2$ orbital [255]. This result is qualitatively in agreement with the crystal structure depicted in figure 13. In fact, moving along [100] or [010] directions of K_2MgF_4 the first neighbour of a F^{-} ligand is a *divalent* Mg^{2+} ion while along the [001] direction the corresponding neighbour is a *monovalent* K^{+} ion.

For understanding why in K_2MgF_4:Ni^{+} $3z^2 - r^2$ becomes the lowest level it is crucial to take into account the role of the 4s orbital enhanced by a significant lessening of the 3d–4s separation on passing from free Cu^{2+} (7.5 eV) to free Ni^{+} (2.5 eV) [130]. By virtue of this fact, the $3z^2 - r^2$ orbital (but not $x^2 - y^2$) can be mixed with the 4s one (figure 12). This admixture produces a decrement of the energy of the lowest level, helping to locate the $3z^2 - r^2$ level below the $x^2 - y^2$ one [127].

Another clue to the present problem comes from the elastic anisotropy associated with the layered structure of K_2MgF_4 and K_2ZnF_4 lattices (figure 13), making the equatorial M^{2+}–F^{-} force constant harder than the axial one. In agreement with this fact the equilibrium geometry of a big closed shell impurity (like Cd^{2+}) in K_2MgF_4 is not described by $R_{ax} = R_{eq}$ but by $R_{ax} > R_{eq}$ [127]. Therefore, as the ionic radius of the Cu^{2+} ion is bigger than that of

Table 8. Evidence of the off-centre instability in the case of d^9 ions in CaF_2 type lattices and also in $SrCl_2$:Fe^+ derived from experimental EPR and ENDOR data.

	Host lattices			
Impurity	CaF_2	SrF_2	$SrCl_2$	References
Ni^+	Off-centre	Off-centre	Off-centre	[50, 51, 256, 257]
Cu^{2+}	On-centre	Off-centre	Off-centre	[48, 56, 58]
Ag^{2+}	On-centre	On-centre	Off-centre	[48, 49, 261]
Fe^+	—	—	Off-centre	[259, 258]

Mg^{2+} one it can be expected that a Cu^{2+} impurity in the $(3z^2 - r^2)^{1.5}(x^2 - y^2)^{1.5}$ closed shell configuration should exhibit an elongated geometry. Let us designate by R^c_{ax} and R^c_{eq} ($<R^c_{ax}$) the axial and equatorial distances corresponding to the $(3z^2 - r^2)^{1.5}(x^2 - y^2)^{1.5}$ configuration. Keeping this geometry, the gap, Δ, between A_{1g} ($(3z^2 - r^2)^1(x^2 - y^2)^2$ configuration) and B_{1g} ($(3z^2 - r^2)^2(x^2 - y^2)^1$ configuration) can still be positive though $\Delta < \Delta_O$, and thus the ground state can be A_{1g} *although* the equilibrium geometry is elongated [127]. Nevertheless, similarly to what happens in the E ⊗ e JT effect, the transition from $(3z^2 - r^2)^{1.5}(x^2 - y^2)^{1.5}$ to $(3z^2 - r^2)^1(x^2 - y^2)^2$ also affords some additional relaxation of ligands, and so the final R_{ax} and R_{eq} values can be written as

$$R_{ax} = R^c_{ax} + \delta R_{ax}; \qquad R_{eq} = R^c_{eq} + \delta R_{eq}. \tag{50}$$

Due to the separation between $3z^2 - r^2$ and $x^2 - y^2$ levels, the most reasonable way of lessening the total energy is through an additional compression described by $\delta R_{ax} > 0$ and $\delta R_{ax} < \delta R_{eq}$. Thus, this reasoning shows that if $\Delta > 0$ for K_2MF_4:Cu^{2+} (M = Mg, Zn) then the unpaired electron can be in the $3z^2 - r^2$ orbital while the axial and equatorial distances are very close indeed. By contrast, if $\Delta < 0$ (such as happens for K_2MgF_4:Ni^+) then $\delta R_{ax} > 0$ and $\delta R_{ax} > \delta R_{eq}$. In other words, in this situation the influence of V_R and the elastic anisotropy *both* favour an elongated geometry. Calculated R_{ax} and R_{eq} values for K_2MgF_4:Cu^{2+} ($R_{ax} = 1.98$ Å and $R_{eq} = 2.03$ Å) and K_2MgF_4:Ni^+ ($R_{ax} = 2.16$ Å and $R_{eq} = 2.03$ Å) are consistent with a bigger tetragonal distortion in the latter system [127, 255].

The present analysis thus demonstrates that mechanisms *different* from those involved in right E ⊗ e JT systems appear when the host lattice symmetry is reduced from cubic to tetragonal. This conclusion thus concurs with those derived from the analysis of section 4.

6. Off-centre instabilities in the ground state of impurities

The displacement of an impurity out of the expected substitutional position in the lattice is a subtle phenomenon which can modify strongly the local geometry and thus all properties associated with the impurity. This phenomenon appears in well known systems like KCl:Li^+ [59, 150], KBr:Cu^+ [60, 61] and also in some centres in semiconductors [53–55]. Nevertheless, for the sake of clarity this section will be focused on the off-centre motions along ⟨100⟩ directions observed in CaF_2 type lattices containing TM impurities [48–51, 56, 256–261]. In table 8 are gathered the systems where the off-centre instability appears. Results embodied in such a table can hardly be understood through *simple* arguments. For instance, it has often been argued that the off-centre motion is favoured by a small size of the impurity [31]. However, in the CaF_2 host lattice Cu^{2+} and Ag^{2+} impurities remain on-centre [58, 261] while only the monovalent Ni^+ impurity, with a bigger size, undergoes a big off-centre excursion along ⟨100⟩ directions [50, 51]. Experimental evidence of this instability is afforded by the EPR spectrum

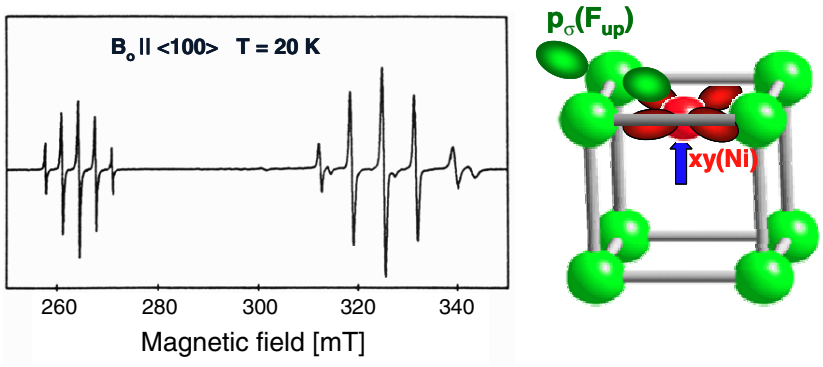

Figure 14. Left: EPR spectrum of CaF_2:Ni^+ taken from [51]. Right: picture of the off-centre motion of the Ni^+ ion showing the overlap between the xy(Ni) and p_σ(F_{up}) orbitals.

taken when **H** is parallel to a ⟨100⟩ direction, showing a superhyperfine interaction of the unpaired electron with *four equivalent* fluorine nuclei (figure 14). Furthermore, additional ENDOR results on CaF_2:Ni^+ [51] have not found any close defect which could be responsible for the instability of the Ni^+ centre.

The results collected in table 8 stress that the off-centre motion cannot *necessarily* be ascribed to a ground state with orbital degeneracy. In fact, ENDOR results on $SrCl_2$:Fe^+ [259] unambiguously prove the existence of an spontaneous off-centre displacement for a cation whose ground state in cubic symmetry is found to be $^4A_2(e_g{}^4t_{2g}^3)$.

The vibrational mode responsible for the off-centre instability in CaF_2 type lattices is the *odd* t_{1u} mode whose components are designated by X, Y and Z. The on-centre situation is described by $X = Y = Z = 0$. Similarly to equation (27), the picture of the ground state energy *just around* the on-centre position is conveyed by [57]

$$H = H_0 + H_{LV}; \qquad H_{LV} = V_X(\mathbf{r})X + V_Y(\mathbf{r})Y + V_Z(\mathbf{r})Z. \tag{51}$$

As the linear vibronic term, H_{LV}, keeps the cubic symmetry, V_Z (**r**) transforms like Z, etc.

Let us denote by $|\Psi^0_{n;j}\rangle$ the wavefunctions corresponding to the ground ($n = 0$) and excited states ($n \geqslant 1$) of the unperturbed Hamiltonian, H_0, where the index j reflects the possible degeneracy. As H_0 is invariant under the inversion centre operation then $\langle\Psi^0_{0;j}|V_\gamma|\Psi^0_{0;k}\rangle = 0$ for $\gamma = X, Y, Z$. This situation is thus quite different from that found in the E ⊗ e JT problem where the equilibrium geometry is essentially determined *only* by the matrix element of H_{LV} within *the frozen* $\{3z^2 - r^2, x^2 - y^2\}$ basis of H_0 [57]. This simple argument also stresses that, *even at the beginning* of the distortion, the admixture of odd excited states of H_0 into the ground one via H_{LV} plays a key role as regards the off-centre instability. That admixture induces rebonding effects as well as a second-order correction to the ground state energy. Thinking for simplicity in a distortion along the OZ axis, this correction to the ground state energy, $\Delta E_{0,j}$, is given by

$$\Delta E_{0,j} = -\sum_{n;l} \frac{|\langle\Psi^0_{0,j}|V_Z(\mathbf{r})|\Psi^0_{n,l}\rangle|^2}{E_n - E_0} Z^2 = -\frac{1}{2}K_V Z^2. \tag{52}$$

This pseudo-JT mechanism [262, 113] produces a softening of the ground state force constant which is thus in competition with the positive force constant

$$K_0 = \left\langle \Psi^0_{0,j} \left| \frac{\partial^2 H_0}{\partial Z^2} \right| \Psi^0_{0,j} \right\rangle \tag{53}$$

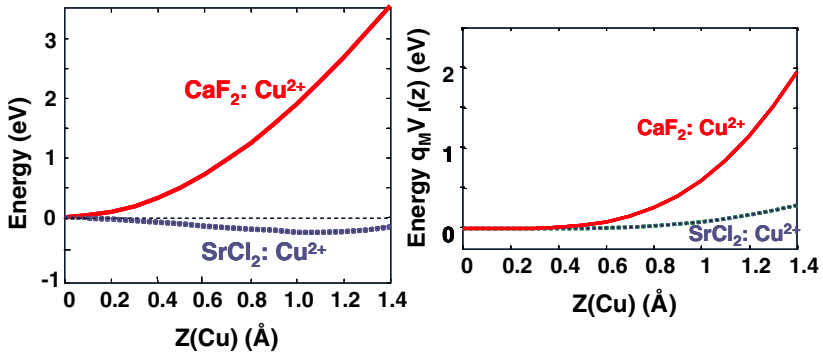

Figure 15. Left: profile of energy for Z movement in Cu^{2+}-doped CaF_2 and $SrCl_2$, obtained by means of DFT calculations. They exhibit a minimum at $Z_0 = 0$ and 1.1 Å, respectively. Right: barrier energy against the off-centre movement, $q_M V_I(Z)$, generated in a simple model of point charges located at lattice sites [57].

involving only the ground state *frozen* wavefunction $|\Psi^0_{0,j}\rangle$. When $K_0 < K_v$ the instability appears, and the curvature of $E(Z)$ at $Z = 0$ becomes negative.

DFT calculations provide reliable information on the behaviour of $E(Z)$ in the neighbourhood of $Z = 0$ but *also* when Z becomes comparable to interatomic distances. This is specially important when the off-centre displacement is characterized by $Z_0 \geqslant 1$ Å because the model based only on the *linear* vibronic interaction (equations (51)–(53)) is obviously not consistent for this goal [52, 57]. As shown in figure 15, DFT calculations on CaF_2:Cu^{2+} and $SrCl_2$:Cu^{2+} reproduce the off-centre instability for both systems (table 8), giving $Z_0 = 0.30$ Å and $Z_0 = 1.10$ Å respectively [57].

A key point for understanding the difference between $SrCl_2$:Cu^{2+} and CaF_2:Cu^{2+} lies in the electrostatic potential on the impurity due to other ions of the lattice. Let us call $V_I(Z)$ such a potential. If we imagine the impurity as a *rigid* ion with charge q_I, the electrostatic energy $q_I V_I(Z)$ increases when $|Z|$ does (figure 15), thus favouring the on-centre situation. Nevertheless, as $V_I(Z) \sim a^{-1}$ (a is the lattice parameter) this potential barrier is bigger for CaF_2:Cu^{2+} than for $SrCl_2$:Cu^{2+}, thus making easier the off-centre motion for the latter system. Mechanisms for overcoming the $q_I V_I(Z)$ barrier involving changes of chemical bonding are depicted in figure 16. Let us consider a pair of bonding–antibonding orbitals both belonging to the same label when $Z \neq 0$, the symmetry group being C_{4v}. As the Z coordinate transforms like A_1 in C_{4v} symmetry, just around $Z = 0$ H_{LV} decreases (increases) the energy of the bonding (antibonding) orbital (figure 16). Therefore, a decrement of the electronic energy can be achieved if the antibonding level is *not fully* populated. Relevant antibonding orbitals in this problem are $b_1(xy)$ and $e(xz, yz)$ coming from t_{2g} in cubic symmetry. As is shown in figure 14, the overlap of the xy orbital with ligand wavefunctions is favoured by the off-centre excursion. Therefore, if the number of electrons in the antibonding $b_1(xy)$ level is less than two this favours the off-centre motion. Moreover, DFT calculations reveal that a decrease of the population of the latter orbital actually enhances the off-centre instability [263].

It has recently been pointed out that unoccupied 4p orbitals can play a relevant role in the off-centre instability of monovalent ions like Fe^+ or Ni^+ [263]. Under C_{4v} symmetry the 4p orbitals are split into $a_1(4p_Z)$ and $e(4p_X; 4p_Y)$. The unoccupied $e(4p_X; 4p_Y)$ orbitals can interact through the H_{LV} operator with antibonding and bonding levels of the same label lying below, leading to a decrease of the electronic energy. In accord with this view, DFT calculations confirm [263] that an increase of the population of antibonding $e(xz, yz)$ levels does favour the

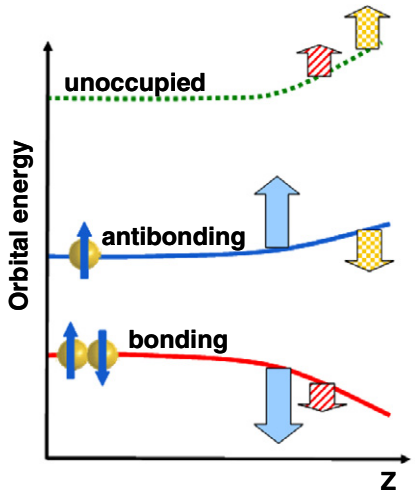

Figure 16. Simple scheme of the pseudo-JT interactions between three orbitals of the same symmetry: fully occupied bonding, half-occupied antibonding and unoccupied antibonding. Big arrows of the same type represent the vibronic interactions between pairs of orbitals.

off-centre motion in $SrCl_2$:Fe^+. It is worth noting that the 3d–4p separation for free Cu^{2+} ions is about 15 eV, while it is only about 5 eV and 6 eV for free Fe^+ and Ni^+ ions, respectively [130]. Therefore, the source of instability coming from 4p orbitals is certainly more important for monovalent ions than for Cu^{2+}. This circumstance together with a lower $q_I V_I(Z)$ barrier make the off-centre motion easier in CaF_2:Ni^+ than in CaF_2:Cu^{2+} [52, 57].

A reduction of the lattice parameter a induced by an applied pressure enhances the electrostatic barrier due to $V_I(Z)$ and thus goes against the off-centre motion. Evidence of the decrease of Z_0 under a hydrostatic pressure has been found for SrF_2:Cu^{2+} [56].

7. Instabilities in excited states of impurities: the Stokes shift

The equilibrium geometry of small molecules and also of impurities embedded in insulators depends on the nature of the electronic state. For an octahedral complex, the transition from the ground to an excited state can change the impurity–ligand distance, but also the local equilibrium geometry [59, 95, 262, 264] due to the interaction with symmetric and non-symmetric local or resonant modes [169, 265–267]. This local relaxation is responsible for the Stokes shift, which is equal to 9000 cm^{-1} for the 4f → 5d transition of $BaLiF_3$:Ce^{3+} [268] but lies in the region 2000–3000 cm^{-1} for Cr^{3+} in halides [21–26, 85, 269]. This section is focused on impurities like Cr^{3+}, Mn^{2+} or Ni^{2+} placed in cubic halide lattices with an octahedral coordination. In these cases, the first excited state responsible for the luminescence is an orbital triplet T_{1g} or T_{2g} [83, 18, 20–26, 270]. Let us first consider the coupling of the excited state only with the symmetric a_{1g} mode (figure 17). If R_g is the equilibrium impurity–ligand distance in the ground state, the adiabatic energy of the ground, E_g, and an excited state, E_{ex}, can be modelled by [59, 95, 183]

$$E_g = (1/2)M_L\omega_a^2 Q_a^2; \qquad E_{ex} = E_{ex}^0 + V_a Q_a + (1/2)M_L\omega_a^2 Q_a^2; \qquad Q_a = \sqrt{6}(R - R_g). \tag{54}$$

A non-zero value of the coupling constant with the a_{1g} mode, V_a, implies that the impurity is *no longer stable* in the ground state geometry once the excited state is reached. According

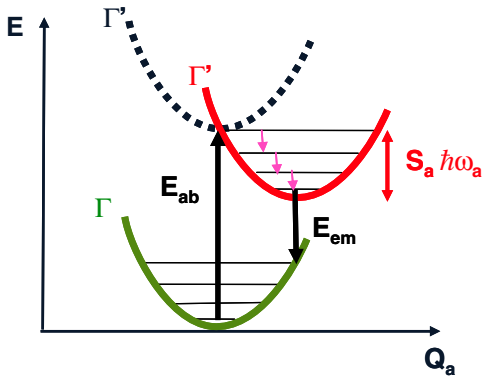

Figure 17. Simple scheme showing the energies of the ground state, Γ, and one excited state, Γ′, as a function of the normal coordinate corresponding to the fully symmetric a_{1g} mode, Q_a. For the excited state, two energy surfaces are depicted, corresponding to an unrelaxed (dashed line) and the actual relaxed state (solid line). Vertical absorption and emission electronic transitions are also shown.

to the Frank–Condon principle, the energy of absorption, E_{abs}, and emission, E_{emis}, maxima is thus given by

$$E_{abs} = E^0_{ex}; \qquad E_{emis} = E^0_{ex} - E_S(a); \qquad E_S(a) = 2S_a\hbar\omega_a = V_a^2/M_L\omega_a^2. \tag{55}$$

Here S_a is the Huang–Rhys factor of the a_{1g} mode and $E_S(a)$ the corresponding contribution to the Stokes shift. When $S_a > 0.1$ direct information on S_a can be derived from low-temperature absorption or emission spectra, where vibrational progressions separated by $\hbar\omega_a$ are sometimes well observed [21–25, 270, 271]. An orbital triplet state can also be *linearly* coupled to the e_g *stretching* local mode (figure 10). Working in the $\{xz, yz, xy\}$ basis of the triplet T state, this coupling is pictured by the following effective Hamiltonian [229, 262]:

$$H_{eff} = V_e(\mathbf{W}_\theta Q_\theta + \mathbf{W}_\varepsilon Q_\varepsilon). \tag{56}$$

In this case the two $3 * 3$ matrices $\mathbf{W}_\theta$ and $\mathbf{W}_\varepsilon$ are both diagonal.

$$\mathbf{W}_\theta = \begin{pmatrix} 1/2 & 0 & 0 \\ 0 & 1/2 & 0 \\ 0 & 0 & -1 \end{pmatrix}; \qquad \mathbf{W}_\varepsilon = \begin{pmatrix} -\sqrt{3}/2 & 0 & 0 \\ 0 & -\sqrt{3}/2 & 0 \\ 0 & 0 & 0 \end{pmatrix}. \tag{57}$$

Once the coupling with the e_g mode is incorporated, the Stokes shift, E_S, can be written:

$$E_S = E_{abs} - E_{emis} = E_S(a) + E_S(e);\ E_S(e) = 2S_e\hbar\omega_e = V_a^2/M_L\omega_e^2. \tag{58}$$

It is worth noting that the coupling with the non-symmetric JT mode does not modify the shape of an optical transition from a singlet to a triplet state [62]. Nevertheless, it produces in low-temperature optical spectra vibrational progressions *additional* to those coming from the a_{1g} mode [21–25].

Let us take as a guide the $^4A_2 \rightarrow {}^4T_2$ transition for d^3 ions in O_h or T_d symmetry, whose energy is equal to $10Dq$ [83]. For this case the coupling constant V_a just reflects the sensitivity of $10Dq$ to R variations, and thus, according to equations (9) and (54), it can be expressed as

$$V_A = \frac{\partial E_{ex}}{\partial Q_A} = \frac{1}{\sqrt{N_L}}\left(\frac{\partial 10Dq}{\partial R}\right)_{R_g} = -\frac{1}{\sqrt{N_L}} n \frac{10Dq}{R_g} \tag{59}$$

where N_L denotes the number of ligands [183, 178]. For CrF_6^{3-} complexes embedded in fluoroelpasolite lattices, taking $10Dq = 16\,000\ cm^{-1}$, $\hbar\omega_a = 560\ cm^{-1}$ and $n = 5$, there

is obtained $V_a = 160\ cm^{-1}$, $S_a = 1.3$ and $E_S(a) = 1400\ cm^{-1}$ [183]. The contribution of the JT mode to the Stokes shift, $E_S(e)$, is found to be quite similar to $E_S(a)$ for CrF_6^{3-} and also MnF_6^{4-} units in fluorides [63, 168, 181]. Therefore, experimental values of E_S around $2700\ cm^{-1}$ for CrF_6^{3-} can reasonably be accounted for through the coupling with a_{1g} and e_g stretching modes. In comparison with results for Cr^{3+} in halides, a small $S_a = 0.2$ value has been reported for the $^3A_2 \rightarrow {}^3T_2$ transition of CrO_4^{4-} [272]. This surprising result for a $10Dq$ dependent transition partially reflects a big value of $\hbar\omega_a$ close to $800\ cm^{-1}$ [273].

The Stokes shift is strongly connected with the quenching of luminescence through the Λ parameter defined by [59, 128]

$$\Lambda = \frac{E_S}{2E_{ex}^0}. \tag{60}$$

As a decrease of Λ favours the appearance of luminescence [128, 39, 168] it is relevant to know how the Stokes shift and Huang–Rhys factors are influenced by pressure [181, 183, 274, 175]. Let us write the R dependence of a local vibrational frequency ω_j ($j = a, e$) as

$$\frac{\partial L\omega_j}{\partial LV} = \frac{1}{3}\frac{\partial L\omega_j}{\partial LR} = -\gamma_j; \qquad (j: a, e). \tag{61}$$

According to equations (9), (55), (59) and (61), the dependence of S_a and $E_S(a)$ on the impurity–ligand distance is just given by [183]

$$S_a \propto R^{9\gamma_a - 2(n+1)}; \qquad E_S(a) \propto R^{6\gamma_a - 2(n+1)}. \tag{62}$$

Equation (62) implies that if $n \leqslant 5$ then S_a should increase upon increasing R, provided the local Grüneisen constant, γ_a, is higher than 1.3. As stretching modes usually exhibit Grüneisen constants close to 2, it can reasonably be expected that S_a decreases when pressure is applied. This statement has been verified for $Cs_2NaScCl_6$:Cr^{3+} under hydrostatic pressure [23] and also for VCl_6^{4-} complexes subject to two different chemical pressures coming from $MgCl_2$ and $CdCl_2$ host lattices [275].

In accordance with equation (62), an increase of $E_S(a)$ when R increases requires $\gamma_a \geqslant 2$, a condition which seems hard to be fulfilled. However, the experimental Stokes shift of MnF_6^{4-} complexes in cubic fluoroperovskites is found to increase with R [180]. Bearing in mind that for the first excited state of MnF_6^{4-} $E_{ex}^0 \approx 6B + 5C - 10Dq$ [83] this quantity also increases with R. For this reason Λ is found to be practically constant along the series [180, 168]. An analysis of experimental E_S values along the whole series indicates that γ_a or γ_e is close to 3 [168], which is not easy to be justified if experiments are carried out under a hydrostatic pressure. Nevertheless, this puzzling situation can reasonably be explained if the variations of E_S are induced by a chemical pressure. If the complex is elastically coupled to the host lattice (figure 5), then ω_a and ω_e can be modified simply by changing the host lattice and thus modifying the k' force constant. By contrast, if the same lattice is kept the force constants k and k' are unmodified under a hydrostatic pressure *if only* the harmonic approximation is considered. This simple reasoning emphasizes that hydrostatic and chemical pressures are no longer equivalent as far as vibrational properties of complexes (elastically coupled to the host lattice) are concerned [168]. This statement is well supported by *ab initio* calculations which confirm a value $\gamma_e = 3$ for MnF_6^{4-} complexes under a chemical pressure, while for $KMgF_3$:Mn^{2+} under a hydrostatic pressure it is found that $\gamma_a = 1.3$ and $\gamma_e = 1.8$ [181]. As a salient feature, calculations reveal that $k'/k \approx 2.5$ and thus MnF_6^{4-} complexes are significantly elastically coupled to the fluoroperovskite lattice. This situation is comparable to that described in section 5.1.3 for systems like MgO:Cu^{2+}: in both cases the host cation and the impurity ion have the same nominal charge and thus, in view of the crystal structure, an important elastic

coupling of the complex to the host lattice can be expected. A quite different situation appears for cubic elpasolite lattices like K_2NaAlF_6 doped with Cr^{3+}, where $k'/k \approx 0.35$ [26]. This is consistent with the fact that the closest AlF_6^{3-} octahedra are well separated by monovalent Na^+ ions and do not share any ligand [170].

The vibronic wavefunctions associated with (56) and (57) are [229]

$$|\Phi_{YZ}\rangle = |yz\rangle|\chi(2\pi/3)\rangle; \qquad |\Phi_{XZ}\rangle = |xz\rangle|\chi(4\pi/3)\rangle; \qquad |\Phi_{XY}\rangle = |xy\rangle|\chi(0)\rangle. \tag{63}$$

Thus, at variance with what is found in (38) for the E ⊗ e Jahn–Teller problem, the wavefunctions involved in (63) are orthogonal. Nevertheless, if we consider an off-diagonal matrix element like $\langle\Phi_{YZ}|L_Z|\Phi_{XZ}\rangle$ involving a purely electronic operator one can write

$$\langle\Phi_{YZ}|L_Z|\Phi_{XZ}\rangle = \langle yz|L_Z|xz\rangle\langle\chi(2\pi/3)|\chi(4\pi/3)\rangle; \langle\chi(2\pi/3)|\chi(4\pi/3)\rangle = \mathrm{e}^{-\frac{3}{2}S_\mathrm{e}}. \tag{64}$$

Equation (64) thus accounts for the vibronic reduction of the spin–orbit coupling in an orbital triplet state. This important reduction was discovered by Ham [229, 276] and later verified experimentally by looking at the spin–orbit splitting of the zero-phonon line [276, 264, 21]. From the present discussion, an increase of the applied pressure would favour an increase of S_e and thus a bigger spin–orbit splitting. No experimental verification of this assertion has been reported up to now.

In agreement with (55), S_a and $E_\mathrm{S}(\mathrm{a})$ depend on the coupling constant V_a, which in turn is proportional to $\mathrm{d}(10Dq)/\mathrm{d}R$ (equation (57)). The analysis afforded in section 3.2.3 emphasizes the subtle origin of the R dependence of $10Dq$. Taking as a guide the CrF_6^{3-} complex, the values of the exponent n and $10Dq$ itself were found to depend strongly on the *small* admixture of ligand 2s wavefunctions into the antibonding e_g orbital [93, 208]. Calculations where the 2s wavefunctions have been suppressed from the basis set have led to a decrement of at least one order of magnitude for S_j and $E_\mathrm{S}(\mathrm{j})$ quantities ($j = \mathrm{a}, \mathrm{e}$) [93].

Acknowledgment

Partial support by the Spanish Ministerio de Educación y Ciencia under Projects BFM2002-01730 and MAT2005-00107 is acknowledged.

References

[1] Blasse G and Grabmaier B C 1994 *Luminescent Materials* (Berlin: Springer)
[2] Powell R C 1998 *Physics of Solid-State Laser Materials* (New York: Springer)
[3] Nikl M 2000 *Phys. Status Solidi* a **178** 595
[4] Babin V, Krasnikov A, Nikl M, Nitsch K, Stolovits A and Zazubovich S 2003 *J. Lumin.* **101** 219
[5] Dorenbos P 2005 *Phys. Status Solidi* a **202** 195
[6] Secu M, Schweizer S, Rogulis U and Spaeth J-M 2003 *J. Phys.: Condens. Matter* **15** 2061
[7] Corradi G, Secu M, Schweizer S and Spaeth J-M 2004 *J. Phys.: Condens. Matter* **16** 1489
[8] Kodama N, Sasaki N, Yamaga M and Masui Y 2001 *J. Lumin.* **19** 94
[9] Nassau K 1983 *The Physics and Chemistry of Colour* (New York: Wiley)
[10] Burns R G 1993 *Mineralogical Applications of Crystal Field Theory* (Cambridge: Cambridge University Press)
[11] Nassau K 2003 *The Science of Color* ed S K Shevell (Amsterdam: Elsevier)
[12] Einstein A 1956 *Investigations on the Theory of the Brownian Movement* (Dover: New York)
[13] Ma S K 1993 *Statistical Mechanics* (Singapore: World Scientific)
[14] Kittel C 2005 *Introduction to Solid State Physics* (New York: Wiley)
[15] Knox K, Shulman R G and Sugano S 1963 *Phys. Rev.* **130** 512
[16] Hall T P P, Hayes W, Stevenson R W H and Wilkens J 1963 *J. Chem. Phys.* **38** 1977
[17] Rousseau J J, Leble A and Fayet J C 1978 *J. Physique* **39** 1215
[18] Rodríguez F and Moreno M 1986 *J. Chem. Phys.* **84** 692
[19] Barriuso M T, Aramburu J A and Moreno M 1999 *J. Phys.: Condens. Matter* **11** L525

[20] Villacampa B, Cases R, Orera V M and Alcalá R 1994 *J. Phys. Chem. Solids* **55** 263
[21] Knochenmuss R, Reber C, Rajasekharan M V and Gudel H U 1986 *J. Chem. Phys.* **85** 4280
[22] Marco de Lucas C, Rodriguez F, Dance J M, Moreno M and Tressaud A 1991 *J. Lumin.* **48/49** 553
[23] Wenger O S, Valiente R and Güdel H U 2001 *J. Chem. Phys.* **115** 3819
[24] Wein G R, Hamilton D S, Sliwczuk U, Rinzler A G and Bartram R H 2001 *J. Phys.: Condens. Matter* **13** 2363
[25] Tanner P A 2004 *Chem. Phys. Lett.* **388** 488
[26] Aramburu J A, Moreno M, Doclo K, Daul C and Barriuso M T 1999 *J. Chem. Phys.* **110** 1497
[27] Helmholtz L 1960 *J. Chem. Phys.* **32** 302
[28] Neuenschwander K, Güdel H U, Collingwood J C and Schatz P N 1983 *Inorg. Chem.* **22** 1712
[29] Dance J M, Grannec J, Tressaud A and Moreno M 1992 *Phys. Status Solidi* b **173** 579
[30] Aramburu J A, Paredes J I, Barriuso M T and Moreno M 2000 *Phys. Rev.* B **61** 6525
[31] Bill H 1984 *The Dynamical Jahn–Teller Effect in Localized Systems* ed Yu E Perlin and M Wagner (Amsterdam: Elsevier)
[32] Vercammen H, Schoemaker D, Briat B, Ramaz F and Callens F 1999 *Phys. Rev.* B **59** 11286
[33] Barriuso M T, García-Fernandez P, Aramburu J A and Moreno M 2001 *Solid State Commun.* **120** 1
[34] Minner E, Lovy D and Bill H 1993 *J. Chem. Phys.* **99** 6378
[35] Boatner L A, Reynolds R W, Abraham M M and Chen Y 1973 *Phys. Rev. Lett.* **31** 7
[36] Badalyan A G, Baranov P G, Vikhnin V S and Khramtson V A 1986 *JETP Lett.* **44** 110
[37] Barriuso M T, Baranov P G and Moreno M 1991 *Radiat. Eff. Defects Solids* **119–121** 177
[38] Soethe H, Vetrov V A and Spaeth J M 1992 *J. Phys.: Condens. Matter* **4** 7927
[39] Marco de Lucas M C, Moreno M, Rodríguez F and Baranov P G 1996 *J. Phys.: Condens. Matter* **8** 2457
[40] Gehloff W and Ulrici W 1980 *Phys. Status Solidi* b **102** 11
[41] Spaeth J-M, Niklas J R and Bartram R H 1992 *Structural Analysis of Point Defects in Solids* (Berlin: Springer)
[42] Hall J L and Schumacher R T 1962 *Phys. Rev.* **127** 1892
[43] Spaeth J-M and Koschnick F K 1991 *J. Phys. Chem. Solids* **52** 1
[44] Van de Valk P J and Trappeniers N J 1977 *Chem. Phys. Lett.* **52** 255
[45] Breñosa A G, Moreno M, Rodriguez F and Couzi M 1991 *Phys. Rev.* B **44** 9859
[46] Di Mauro E and Domiciano S M 2001 *Physica* B **304** 398
[47] Aramburu J A and Moreno M 1997 *Phys. Rev.* B **56** 604
[48] Bill H 1973 *Phys. Lett.* A **44** 101
[49] Moreno M 1974 *Ann. Fis.* **70** 261
[50] Casas Gonzalez J, den Hartog H W and Alcalá R 1980 *Phys. Rev.* B **21** 3826
[51] Studzinski P, Casas González J and Spaeth J M 1984 *J. Phys. C: Solid State Phys.* **17** 5411
[52] Aramburu J A, García Fernández P, Barriuso M T and Moreno M 2003 *Phys. Rev.* B **67** 020101
[53] DeLeo G G, Watkins G D and Fowler W B 1988 *Phys. Rev.* B **37** 1013
[54] Chadi D J and Chang K J 1989 *Phys. Rev.* B **39** 10063
[55] Herring C, Johnson N M and Van de Walle C G 2001 *Phys. Rev.* B **64** 125209
[56] Ulanov V A, Krupski M, Hoffmann S K and Zaripov M M 2003 *J. Phys.: Condens. Matter* **15** 1081
[57] García Fernández P, Aramburu J A, Barriuso M T and Moreno M 2004 *Phys. Rev.* B **69** 174110
[58] Ulanov V A, Zaripov M M, Shustov V A and Fazlizhanov I I 2001 *Phys. Solid State* **40** 408
[59] Stoneham A M 1975 *Theory of Defects in Solids: Electronic Structure of Defects in Insulators and Semiconductors* (Oxford: Oxford University Press)
[60] Payne S A 1987 *Phys. Rev.* B **236** 6125
[61] McClure D S and Weaver S C 1991 *J. Phys. Chem. Solids* **52** 81
[62] Toyozawa Y and Inoue M 1966 *J. Phys. Soc. Japan* **21** 1663
[63] Barriuso M T, Aramburu J A and Moreno M 1996 *Phys. Status Solidi* b **196** 193
[64] Pedrini C, McClure D S and Anderson C H 1979 *J. Chem. Phys.* **70** 4959
[65] Dorenbos P 2003 *J. Phys.: Condens. Matter* **15** 2645
[66] Thiel C W, Cruguel H, Sun Y, Lapeyre G J, Macfarlane R M, Equall R W and Cone R L 2001 *J. Lumin.* **94/95** 1
[67] Joubert M F, Kazanskii S A, Guyot Y, Gâcon J C and Pedrini C 2004 *Phys. Rev.* B **69** 165217
[68] Stjern D C, DuVarney R C and Unruh W P 1974 *Phys. Rev.* B **10** 1044
[69] Buzare J Y and Fayet J C 1976 *Phys. Status Solidi* b **74** 393
[70] Buzare J Y and Fayet J C 1977 *Solid State Commun.* **21** 1097
[71] Siegel E and Müller K A 1979 *Phys. Rev.* B **19** 109
[72] Murrieta H, Rubio J and Aguilar G 1979 *Phys. Rev.* B **19** 5516
[73] Wan-Lun Y 1994 *J. Phys.: Condens. Matter* **6** 5105
[74] Aramburu J A, García-Lastra J M, Barriuso M T and Moreno M 2003 *Int. J. Quantum Chem.* **91** 197

[75] Fallin M, Latypov V, Kazakov B, Leushin A, Bill H and Lovy D 2000 *Phys. Rev.* B **61** 9441
[76] García-Lastra J M, Aramburu J A, Barriuso M T and Moreno M 2002 *Radiat. Eff. Defects Solids* **157** 931
[77] Baraldi A, Bertoli P, Capelleti R and Ruffini A 2001 *Phys. Rev.* B **63** 134302
[78] Kohn W 1964 *Phys. Rev.* **133** A171
[79] Resta R 2002 *J. Phys.: Condens. Matter* **14** R625
[80] Souza I 2000 *PhD Thesis* University of Illinois
[81] Martin R M 2004 *Electronic Structure: Basic Theory and Practical Methods* (Cambridge: Cambridge University Press)
[82] Sugano S and Shulman R G 1963 *Phys. Rev.* B **130** 517
[83] Sugano S, Tanabe Y and Kamimura H 1970 *Multiplets of Transition-Metal Ions in Crystals* (New York: Academic)
[84] Moreno M, Aramburu J A and Barriuso M T 2004 *Struct. Bonding* **106** 127
[85] Gilardoni F, Weber J, Bellafrouh K, Daul C and Güdel H U 1996 *J. Chem. Phys.* **104** 7624
[86] Abbet S, Heiz U, Häkkinen H and Landman U 2001 *Phys. Rev. Lett.* **86** 5950
[87] Radzhabov E and Kirm M 2005 *J. Phys.: Condens. Matter* **17** 5821
[88] Stevens F, Van Speybroeck, Pawels E, Vrielinck H, Callens F and Waroquier M 2005 *Phys. Chem. Chem. Phys.* **7** 240
[89] Kohn W 1996 *Phys. Rev. Lett.* **76** 3168
[90] Barkyoumb J H and Mansour A N 1992 *Phys. Rev.* B **46** 8768
[91] Dalba G, Fornasini P, Grisenti R and Purans J 1999 *Phys. Rev. Lett.* **82** 4240
[92] Gaudry E, Kiratisin A, Sainctavit P, Brouder C, Mauri F and Ramos A 2003 *Phys. Rev.* B **67** 094108
[93] Moreno M, Aramburu J A and Barriuso M T 1997 *Phys. Rev.* B **56** 14423
[94] García-Fernandez P, Bersuker I, Aramburu J A, Barriuso M T and Moreno M 2005 *Phys. Rev.* B **71** 184117
[95] Lannoo M and Bourgoin J 1981 *Point Defects in Semiconductors I* (Berlin: Springer)
[96] Solomon E I 2001 *Inorg. Chem.* **40** 3656
[97] Zaanen J, Sawatzky G A and Allen J W 1985 *Phys. Rev. Lett.* **55** 418
[98] Arima T, Tokura Y and Torrance J B 1993 *Phys. Rev.* B **48** 17006
[99] Pollini I, Mosser A and Parlebas J C 2001 *Phys. Rep.* **355** 1
[100] Slater J C 1963 *Quantum Theory of Molecules and Solids* (New York: McGraw-Hill)
[101] Drickamer H G and Frank C W 1973 *Electronic Transitions and the High Pressure Chemistry of Solids* (London: Chapman and Hall)
[102] Bocquet A E, Saitoh T, Mizokawa T and Fujimori A 1992 *Solid State Commun.* **83** 11
[103] Ogasawara K, Iwata T, Koyama Y, Ishii T, Tanaka I and Adachi H 2001 *Phys. Rev.* B **64** 115413
[104] de Graaf C, Illas F, Broer R and Nieuwpoort W C 1997 *J. Chem. Phys.* **106** 3287
[105] Moreira I P R, Illas F, Calzado C J, Sanz J F, Malrieu J P, Ben Amor N and Maynau D 1999 *Phys. Rev.* B **59** R6593
[106] Babel D and Tresaud A 1985 *Inorganic Solid Fluorides* ed P Hagenmuller (New York: Academic)
[107] Reinen D and Friebel C 1979 *Struct. Bonding* **37** 1
[108] Reinen D and Atanasov M 1991 *Magn. Reson. Rev.* **15** 167
[109] Van den Brink J, Khaliullin G and Khomskii D 2002 *Colossal Magnetoresistive Manganites* ed T Chatterij (Dordrecht: Kluwer) (*Preprint* cond-mat/0206053)
[110] Grochala W and Hoffman R 2001 *Angew. Chem. Int. Edn* **40** 2743
[111] Bersuker I 1995 *Ferroelectrics* **164** 5
[112] Akberzadeh A R, Bellaiche L, Leung K, Iñiguez J and Vanderbilt D 2004 *Phys. Rev.* B **70** 054103
[113] Bersuker I 2006 *The Jahn–Teller Effect* (Cambridge: Cambridge University Press)
[114] Millis A J, Shraiman B I and Mueller R 1996 *Phys. Rev. Lett.* **77** 175
[115] Millis A J 1998 *Nature* **392** 147
[116] Khomskii D I and Kugel K I 2003 *Phys. Rev.* B **67** 134401
[117] Kabanov V V and Mihailovic D 2002 *Phys. Rev.* B **65** 212508
[118] Tachiki M, Machida M and Egami T 2003 *Phys. Rev.* B **67** 174506
[119] Chiu Y-N 1997 *Phys. Rev.* B **55** 6022
[120] Song K S and Williams R T 1999 *Self-Trapped Excitons* (Berlin: Springer)
[121] Laredo E, Rowan L G and Slifkin L 1981 *Phys. Rev. Lett.* **47** 384
[122] Bennebroek M T 1996 *PhD Thesis* University of Leiden
[123] Houlier B 1975 *Solid State Commun.* **17** 263
[124] Laguta V V, Rosa J, Zaritskii M I, Nikl M and Usuki Y 1998 *J. Phys.: Condens. Matter* **10** 7293
[125] Laguta V V, Vedda A, Di Martino D, Martini M, Nikl M, Mihóková E, Rosa J and Usuki Y 2005 *Phys. Rev.* B **71** 235108

[126] Alcalá R, Zorita E and Alonso P J 1988 *J. Phys. C: Solid State Phys.* **21** 461
[127] García-Lastra J M, Aramburu J A, Barriuso M T and Moreno M 2004 *Phys. Rev. Lett.* **93** 226402
[128] Bartram R H and Stoneham M 1975 *Solid State Commun.* **17** 1593
[129] Poole R T, Jenkin J G, Liesegang J and Leckey R C G 1975 *Phys. Rev.* B **11** 5179
[130] Moore C E 1971 *Atomic Energy Levels* (Washington, DC: Nat Stand Ref Pat Ser Nat Bur Stand)
[131] Jörgensen C K 1971 *Modern Aspects of Ligand Field Theory* (Amsterdam: North-Holland)
[132] Barriuso M T and Moreno M 1984 *Phys. Rev.* B **29** 3623
[133] Mortier M, Piriou B, Buzaré J Y, Rousseau M and Gesland J Y 2003 *Phys. Rev.* B **67** 115126
[134] Nistor S V, Schoemaker D and Ursu I 1994 *Phys. Status Solidi* b **185** 9
[135] Aramburu J A, Moreno M, Cabria I, Barriuso M T, Sousa C, de Graaf C and Illas F 2000 *Phys. Rev.* B **62** 13356
[136] Hamilton J F 1988 *Adv. Phys.* **37** 359
[137] Spoonhower J P and Marchetti A P 1990 *J. Phys. Chem. Solids* **52** 793
[138] Bennebroek M T, Poluektov O G, Zakrzewski A J, Baranov P G and Schmidt J 1995 *Phys. Rev. Lett.* **74** 442
[139] Abragam A and Bleaney B 1970 *Electron Paramagnetic Resonance of Transition Metal Ions* (London: Oxford University Press)
[140] Lever A B P 1985 *Inorganic Electronic Spectroscopy* (Amsterdam: Elsevier)
[141] Weil J A, Bolton J R and Wertz J E 1994 *Electron Paramagnetic Resonance* (New York: Wiley)
[142] Simonetti J and McClure D S 1979 *J. Chem. Phys.* **71** 795
[143] Hirako S and Onaka R 1982 *J. Phys. Soc. Japan* **51** 1255
[144] García Fernandez P, Barriuso M T, Aramburu J A and Moreno M 2003 *Chem. Phys. Lett.* **374** 151
[145] Pollini I 1994 *Phys. Rev.* B **50** 2095
[146] de Viry D, Casalboni M, Palumno M and Zema N 1990 *Solid State Commun.* **76** 1051
[147] Aramburu J A, Barriuso M T and Moreno M 1996 *J. Phys.: Condens. Matter* **8** 6901
[148] Van der Kolk E, Dorenbos P, van Eijk C W E, Vink A P, Weil M and Chaminade J P 2004 *J. Appl. Phys.* **95** 7867
[149] Bruce Chase D and McClure D S 1976 *J. Chem. Phys.* **64** 74
[150] Farge Y and Fontana M 1974 *Perturbations Electroniques et Vibrationelles Localisées dans les Solides Ioniques* (Paris: Masson)
[151] Sliwczuk U, Bartram R H, Gabbe D R and McCollum B C 1991 *J. Phys. Chem. Solids* **52** 357
[152] Couzi M, Moreno M and Breñosa A G 1994 *Solid State Commun.* **91** 481
[153] Silversmith A J and Macfarlane R M 1992 *Phys. Rev.* B **45** 5811
[154] Aramburu J A and Moreno M 1985 *J. Chem. Phys.* **83** 6071
[155] Miyanaga T 1979 *J. Phys. Soc. Japan* **4** 167
[156] Yamaga M, Hayashi Y and Yoshioka H 1979 *J. Phys. Japan* **4** 677
[157] Aramburu J A and Moreno M 1986 *Solid State Commun.* **58** 305
Aramburu J A and Moreno M 1987 *Solid State Commun.* **62** 513
[158] Lacroix R and Emch G 1962 *Helv. Phys. Acta* **35** 1962
[159] Misetich A A and Watson R E 1966 *Phys. Rev.* B **143** 335
[160] Aramburu J A and Moreno M 1983 *J. Chem. Phys.* **79** 4993
[161] Zheng W C, Wu X X, Zhou Q and Mei Y 2005 *Chem. Phys. Lett.* **406** 192
[162] Moreno M 1990 *J. Phys. Chem. Solids* **51** 835
[163] Moreno M and Barriuso M T 1990 *Solid State Commun.* **75** 133
[164] Vértes A, Korecz L and Burger K 1979 *Mössbauer Spectroscopy* (Amsterdam: Elsevier)
[165] Villacampa B, Alcalá R, Alonso P J, Moreno M, Barriuso M T and Aramburu J A 1994 *Phys. Rev.* B **49** 1039
[166] Barriuso M T, Aramburu J A and Moreno M 2001 *J. Mol. Struct. (THEOCHEM)* **537** 117
[167] Luaña V, Bermejo M, Flórez M, Recio J M and Pueyo L 1989 *J. Chem. Phys.* **90** 6409
[168] Barriuso M T, Moreno M and Aramburu J A 2002 *Phys. Rev.* B **65** 064441
[169] Sturge M D 1971 *Solid State Commun.* **9** 899
[170] Flerov I N, Gorev M V, Aleksandrov K S, Tressaud A, Grannec J and Couzi M 1998 *Mater. Sci. Eng.* R **24** 81
[171] García-Fernández P, Sousa C, Aramburu J A, Barriuso M T and Moreno M 2005 *Phys. Rev.* B **72** 155107
[172] Kosevich A M, Lifshitz E M, Landau L D and Pitaevskii L P 2002 *Theory of Elasticity* (Oxford: Butterworth-Heinemann)
[173] Duclos S J, Vohra Y K and Ruoff A L 1990 *Phys. Rev.* B **41** 5372
[174] Chen W, Li G, Malm J O, Huang Y, Wallenberg R, Han H, Wang Z and Bovin J O 2000 *J. Lumin.* **91** 139
[175] Bray K L 2001 *Top. Curr. Chem.* **213** 1
[176] Drickamer H G 1967 *J. Chem. Phys.* **47** 1880
[177] Hernández D, Rodríguez F, Moreno M and Güdel H U 1999 *Physica* B **265** 186
[178] Dolan J F, Rinzler A G, Kappers L A and Bartram R H 1992 *J. Phys. Chem. Solids* **53** 905

[179] Woods A M, Sinkovits R S, Charpie J C, Huang W L, Bartram R H and Rossi A R 1993 *J. Phys. Chem. Solids* **54** 543
[180] Marco de Lucas M C, Rodriguez F and Moreno M 1994 *Phys. Rev.* B **50** 2760
[181] García-Lastra J M, Wesolowski T, Barriuso M T, Aramburu J A and Moreno M 2006 *J. Phys.: Condens. Matter* **18** 1519
[182] Jahren A H, Kruger M B and Jeanloz R 1992 *J. Appl. Phys.* **71** 1579
[183] Moreno M, Barriuso M T and Aramburu J A 1992 *J. Phys.: Condens. Matter* **4** 9481
[184] Rogulis U, Spaeth J-M, Cabria I, Moreno M, Aramburu J A and Barriuso M T 1998 *J. Phys.: Condens. Matter* **10** 6473
[185] Zorita E, Alonso P J, Alcalá R, Spaeth J M and Soethe H 1988 *Solid State Commun.* **66** 773
[186] Barriuso M T and Moreno M 1982 *Phys. Rev.* B **26** 2271
[187] Aoki H, Arakawa M and Yosida T 1983 *J. Phys. Soc. Japan* **52** 2216
[188] Yosida T, Aoki H, Takeuchi H, Arakawa M and Horai K 1991 *J. Phys. Soc. Japan* **60** 625
[189] Cabria I, Moreno M, Aramburu J A, Barriuso M T, Rogulis U and Spaeth J-M 1998 *J. Phys.: Condens. Matter* **10** 6481
[190] Atanasov M, Brunold T C, Güdel H U and Daul C 1998 *Inorg. Chem.* **37** 4589
[191] Ishii T, Ogasawara K and Adachi H 2001 *J. Chem. Phys.* **115** 492
[192] Wissing K, Barriuso M T, Aramburu J A and Moreno M 1999 *J. Chem. Phys.* **111** 10217
[193] Seth M and Ziegler T 2005 *J. Chem. Phys.* **123** 144105
[194] Stückl A C, Daul C A and Güdel H U 1997 *J. Chem. Phys.* **107** 4606
[195] Ziegler T, Rauk A and Baerends E J 1976 *Chem. Phys.* **16** 209
[196] Emery J, Leble A and Fayet J C 1981 *J. Phys. Chem. Solids* **9** 789
[197] Emery J and Fayet J C 1982 *Solid State Commun.* **42** 683
[198] Flórez M, Seijo L and Pueyo L 1986 *Phys. Rev.* B **34** 1200
[199] Barriuso M T, Aramburu J A, Moreno M, Flórez M, Fernández Rodrigo G and Pueyo L 1988 *Phys. Rev.* B **38** 4239
[200] Aramburu J A, Moreno M and Barriuso M T 1992 *J. Phys.: Condens. Matter* **4** 9089
[201] McWeeny R and Sutcliffe B T 1976 *Methods of Molecular Quantum Mechanics* (London: Academic)
[202] Galindo A and Pascual P 1989 *Mecánica Cuántica* (Madrid: Eudema)
[203] Burns G and Axe J 1966 *J. Chem. Phys.* **45** 4362
[204] Bermejo M and Pueyo L 1982 *J. Chem. Phys.* **78** 854
[205] Adachi H, Shiokawa S, Tsukada M and Sugano S 1979 *J. Phys. Soc. Japan* **47** 1528
[206] Richardson J W and Janssen G 1989 *Phys. Rev.* B **39** 4958
[207] López-Moraza S, Pascual J L and Barandiarán Z 1995 *J. Chem. Phys.* **103** 2117
[208] Moreno M, Barriuso M T and Aramburu J A 1994 *Int. J. Quantum Chem.* **52** 829
[209] Atanasov M, Daul C A and Rauzy C 2003 *Chem. Phys. Lett.* **367** 737
[210] Curie D, Barthou C and Canny B 1974 *J. Chem. Phys.* **61** 3048
[211] Moreno M, Barriuso M T and Aramburu J A 1992 *Appl. Magn. Reson.* **3** 283
[212] Valiente R, Aramburu J A, Barriuso M T and Moreno M 1994 *Int. J. Quantum Chem.* **52** 1051
[213] Vrielinck H, Sabbe K, Callens F and Matthys P 2001 *Phys. Chem. Chem. Phys.* **3** 1709
[214] Steffen G, Reinen D, Stratemeier H, Riley M J, Hitchman M A, Mattthies H E, Recker K, Wallrafen F and Niklas J R 1990 *Inorg. Chem.* **29** 2123
[215] Breñosa A G, Moreno M and Aramburu J A 1991 *J. Phys.: Condens. Matter* **3** 7743
[216] Barriuso M T, Aramburu J A and Moreno M 2002 *J. Phys.: Condens. Matter* **14** 6521
[217] Valiente R, Rodriguez F, Aramburu J A, Moreno M, Barriuso M T, Sousa C and De Graaf C 2002 *Int. J. Quantum Chem.* **86** 239
[218] Du Varney R C, Niklas J R and Spaeth J M 1981 *Phys. Status Solidi* b **103** 329
[219] Jeck R K and Krebs J J 1972 *Phys. Rev.* B **5** 1677
[220] Newman D J and Ng B 1989 *Rep. Prog. Phys.* **52** 694
[221] Barandiarán Z and Pueyo L 1983 *J. Chem. Phys.* **79** 1926
[222] Pierloot K, Van Praet E and Vanquickenborne L G 1992 *J. Chem. Phys.* **96** 4163
[223] Breñosa A G, Rodriguez F and Moreno M 1988 *J. Phys. C: Solid State Phys.* **21** L623
[224] Gaudry E 2004 *PhD Thesis* Université Paris
[225] Canny B, Chervin J C, Curie D, González J, Berry D and Ho S A 1987 *Spectroscopy of Solid-State Laser-Type Materials* (Geneva: Etore Majorana International Science Series)
[226] Orgel L E 1957 *Nature* **179** 1348
[227] García-Lastra J M, Barriuso M T, Aramburu J A and Moreno M 2005 *Phys. Rev.* B **72** 113104
[228] Shen Y R, Grinberg M, Barzowska J, Bray K L, Hanuza J and Deren P J 2006 *J. Lumin.* **116** 1

[229] Ham F S 1972 *Electron Paramagnetic Resonance* ed S Geschwind (New York: Plenum)
[230] García-Lastra J M, Barriuso M T, Aramburu J A and Moreno M 2005 *Chem. Phys.* **317** 103
[231] Öpik U and Pryce M H M 1957 *Proc. R. Soc.* A **238** 425
[232] O'Brien M C M 1964 *Proc. R. Soc.* A **281** 323
[233] Stoneham A M 2005 *Phys. Status Solidi* c **2** 25
[234] Burton W K, Cabrera N and Frank F C 1951 *Phil. Trans. R. Soc.* A **243** 299
[235] Coffman R E 1966 *Phys. Lett.* **21** 381
[236] Coffman R E, Lyle D L and Mattison D R 1968 *J. Phys. Chem.* **72** 1392
[237] Tolparov Y N, Bir G L, Sochava L S and Kovalev N N 1974 *Sov. Phys.—Solid State* **16** 573
[238] Monnier A, Gerber A and Bill H 1991 *J. Chem. Phys.* **94** 5891
[239] Herrington J R, Boatner L A, Aton T J and Estle T L 1974 *Phys. Rev.* B **10** 833
[240] Hayes W and Wilkens J 1964 *Proc. R. Soc.* A **281** 340
[241] Barriuso M T, Aramburu J A and Moreno M 1990 *J. Phys.: Condens. Matter* **2** 771
[242] Nurullin G M, Galygo L N, Egranov A V and Nepomnyachikh A I 1991 *J. Phys.: Condens. Matter* **3** 83
[243] Lahoz F, Villacampa B and Alcalá R 1998 *J. Phys. Chem. Solids* **59** 981
[244] Guha S and Chase L L 1974 *Phys. Rev.* B **12** 1658
[245] Schoenberg A, Suss J T, Luz Z and Low W 1974 *Phys. Rev.* B **9** 2047
[246] Riley M J, Hitchman M A and Reinen D 1986 *Chem. Phys.* **102** 11
[247] Augustyniak-Jabłokow M A, Yablokov Y V, Łukaszewicz K, Pietraszko A, Petrashen V E and Ulanov V A 2001 *Chem. Phys. Lett.* **344** 345
[248] Höchli U, Müller K A and Wysling P 1965 *Phys. Lett.* **15** 5
[249] Reynolds W, Boatner L, Abraham M and Chen Y 1974 *Phys. Rev.* B **10** 3802
[250] Hjortsberg A, Nygren B, Vallin J and Ham F S 1977 *Phys. Rev. Lett.* **39** 1233
[251] Tregenna-Piggott Ph L W 2003 *Adv. Quantum Chem.* **44** 446
[252] Pascual J L, Seijo L and Barandiarán Z 1993 *J. Chem. Phys.* **98** 9715
[253] Aguado F, Rodríguez F, Valiente R, Itié J and Munsch P 2004 *Phys. Rev.* B **70** 214104
[254] Alcalá R, Zorita E and Alonso P J 1988 *J. Phys. C: Solid State Phys.* **21** 461
[255] García-Lastra J M, Aramburu J A, Barriuso M T and Moreno M 2004 *Chem. Phys. Lett.* **385** 286
[256] Alonso P J, Casas González J, den Hartog H W and Alcalá R 1983 *Phys. Rev.* B **27** 2722
[257] Alcalá R, Cases R and Alonso P J 1986 *Phys. Status Solidi* b **135** K63
[258] Nistor S V, Stefan M and Schoemaker D 1999 *Phys. Status Solidi* b **214** 228
[259] Ghica H D, Nistor S V, Vrielinck H, Callens F and Schoemaker D 2004 *Phys. Rev.* B **70** 024105
[260] Dance J M, Grannec J, Tressaud A and Hagenmuller P 1988 *C. R. Acad. Sci. Paris* **307** 137
[261] Eremin M V, Ulanov V A and Zaripov M M 1998 *Appl. Magn. Reson.* **14** 435
[262] Bersuker I and Polinger V 1989 *Vibronic Interactions in Molecules and Crystals* (Berlin: Springer)
[263] García-Fernández P, Aramburu J A, Barriuso M T and Moreno M 2006 *Phys. Rev.* B submitted
[264] Solomon E I and McClure D S 1974 *Phys. Rev.* B **9** 4690
[265] Calistru D M, Demos S G and Alfano R R 1997 *Phys. Rev. Lett.* **78** 374
[266] Thurian P, Kaczmarczyk G, Siegle H, Heitz R, Hoffmann A, Broser I, Meyer B K, Hoffbauer R and Scherz U 1995 *Mater. Sci. Forum* **196–201** 1571
[267] Dahan P, Fleurov V, Thurian P, Heitz R, Hoffmann A and Broser I 1998 *Phys. Rev.* B **57** 9690
[268] Marsman M, Andriessen J and van Eijk C W E 2000 *Phys. Rev.* B **61** 16477
[269] Al-Abdalla A, Barandiarán Z and Seijo L 1998 *J. Chem. Phys.* **108** 2005
[270] Rodríguez F, Riesen H and Güdel H U 1991 *J. Lumin.* **50** 101
[271] Jaque F, López F J, Cussó F, Meseguer F, Agulló-López F and Moreno M 1983 *Solid State Commun.* **47** 103
[272] Hazenkamp M F, Güdel H U, Atanasov M, Kesper U and Reinen D 1996 *Phys. Rev.* B **53** 2367
[273] Wissing K, Aramburu J A, Barriuso M T and Moreno M 1998 *Solid State Commun.* **108** 1001
[274] Grinberg M, Barzowska J, Shen Y R, Meltzer R S and Bray K L 2004 *Phys. Rev.* B **69** 205101
[275] Galli B, Hauser A and Güdel H U 1985 *Inorg. Chem.* **24** 2271
[276] Ham F S 2000 *J. Lumin.* **85** 193